Mitigating the Impact of UAV Fluctuations on Air-to-Ground Wireless Communications in the Presence of Channel Aging

A. Regilane L. Paiva, Walter C. Freitas Jr, Yuri C. B. Silva, Roberto P. Antonioli, and Gábor Fodor

***Abstract*—Recent works have pointed out that uncrewed aerial vehicle (UAV) platform fluctuations due to jittering, wobbling and shaking degrade the performance of air-to-ground wireless systems. Similarly, recent works have shown that the air-to-ground wireless channel suffers from the effect of channel aging due to the high mobility of UAVs. Delays inherent to the network, high Doppler frequencies and hardware impairments accentuate this effect, as well as fluctuations in the UAV platform. Unfortunately, the literature still lacks appropriate channel models that take into account the influence of UAV fluctuations on the channel aging autocorrelation function, which is an essential requirement for channel prediction-based mitigation solutions. Therefore, in this paper, we develop autocorrelation functions that are appropriate for evaluating and mitigating the impact of UAV fluctuations on the performance of the air-to-ground channels. We demonstrate that the UAV fluctuations affect the time autocorrelation function of the channel, and consequently the coherence time, exacerbating the effects of channel aging. Furthermore, this effect is accentuated with an increasing distance between the antennas and the centroid of the UAV, and with increasing the carrier frequency. We propose a channel predictor based on an extended Kalman filter and develop autocorrelation functions to mitigate the impact of channel aging with UAV fluctuations on the spectral efficiency (SE). Then, we observe that considering statistical models of UAV fluctuations in the channel predictor design can improve SE.**

***Index Terms*—channel aging, channel prediction, extended Kalman filter, jittering, uncrewed aerial vehicle**

I. Introduction

A. Background

Recently, the industrial and academic communities have focused efforts on the research and development of wireless communication systems that serve the digital airspace, including broadband connectivity services to uncrewed aerial vehicles (UAVs) [1]. As the literature points out [1], [2], [3], [4], to meet the connectivity demands imposed by digital airspace services provided by UAVs, including autonomous delivery, monitoring and inspection, precision agriculture, emergency assistance, surveillance, security, and more, there is a need for improved command, control, and data specifications in communication between UAVs and the serving base stations. These requirements concern factors such as long range, high energy efficiency, low latency, low interference, bandwidth, reliability, security, and others. Meeting these requirements presents challenges for traditional ground-to-UAV communication. Sixth generation (6G) networks serving UAVs offer solutions to meet these requirements [5], [6]. However, due to its characteristics of distributed or co-located massive multiple-input multiple-output (MIMO), an essential requirement for this integration is the acquisition of instantaneous air-to-ground wireless channel state information (CSI) [6], whose inaccuracy impacts the overall performance of the network.

Several factors contribute to errors or imperfections in CSI during the training and estimation stages in massive MIMO systems. For example: spatially uncorrelated channel, reception noise, high mobility, high carrier frequencies and interference [7], in addition to antenna disturbances [8] and scatterers, hardware impairments [9] and delays [10]. Factors such as mobility, antenna disturbances and hardware impairments, prevalent in air-to-ground wireless communications, result in continuous variations of the channel on a small scale, causing the channel samples to decorrelate gradually over time. This gradual decorrelation leads to a mismatch between the CSI and the instantaneous channel response, resulting in the phenomenon of channel aging [11].

For UAV communication, antenna disturbances are fluctuations on the UAV platform caused by jittering, wobbling and shaking, due to wind gusts, adverse weather conditions, interference in the control system, malfunctioning sensors or vibrating rotors/propellers during movement, hovering, takeoff and landing [12], [13], [14]. When antennas are installed on the UAV platform, axis fluctuations (pitch, yaw and roll) induce random attitude variations in the antenna array, making its expected response inaccurate.

Unlicensed millimeter wave (mmWave) bands and hybrid-beamforming architecture have been explored to achieve high-performance as well as low-latency connectivity in network-connected UAVs [1], [15], [16], [17]. However, when com-

A. Regilane L. Paiva, Walter C. Freitas Jr, Yuri C. B. Silva and Roberto P. Antonioli. are with the Wireless Telecom Research Group (GTEL), Federal University of Ceará, Fortaleza 60455-760, Brazil. (e-mail: regislane@gtel.ufc.br, walter@gtel.ufc.br, yuri@gtel.ufc.br, antonioli@gtel.ufc.br). (ORCID: 0009-0004-2748-6458, 0000-0002-0821-3460, 0000-0002-1795-6004, 0000-0003-1163-9953)

Gábor Fodor is with Ericsson Research, 16480 Stockholm, Sweden, and also with the Division of Decision and Control, KTH Royal Institute of Technology, 11428 Stockholm, Sweden (e-mail: gabor.fodor@ericsson.com). (ORCID: 0000-0002-2289-3159)

This study was financed in part by Ericsson Research, Sweden, and Ericsson Innovation Center, Brazil, Technical Cooperation Contract UFC.50, in part by the Coordenação de Aperfeiçoamento de Pessoal de Nível Superior - Brasil (CAPES) - Finance Code 001, in part by CNPq, in part by FUNCAP/Universal Grant UNI-0210-00043.01.00/23, and in part by CNPq/INCT-Signals Grant 406517/2022-3. G. Fodor was partially supported by the Celtic project 6G for Connected Sky, Project ID: C2021/1-9.

Submission: 2023-12-05, First decision: 2024-04-29, Acceptance: 2024-09-18, Publication: 2024-09-21.

Digital Object Identifier: 10.14209/jcis.2024.15

pared to microwaves, mmWave communication links have shorter wavelengths, therefore being more susceptible to loss due to absorption, scattering, and blocking, as well as to variations due to mobility and disturbance of antennas and scatterers. Therefore, it is reasonable to expect that jittering/wobbling will have a significant impact on mmWave communication in network-connected UAVs.

B. Related work

Recent studies, motivated by the inevitable UAV platform fluctuations [12], [13], [14], have evaluated the impacts of jittering/wobbling on UAV communication [18], [19], [20], [21], highlighting that these effects significantly interfere in network management and optimization operations, such as: energy efficiency, power allocation, security, channel estimation, beam management and sensing. These observations motivate research into modeling and analyzing the effects of jittering/wobbling on the correlation function of aerial wireless channels.

In [22], the authors conduct an analytical study of UAV-based mmWave line of sight (LoS) links under hovering Gaussian fluctuations. They employ antenna directivity gain and beam misalignment as a strategy to mitigate UAV fluctuation errors. Correlation function models based on geometry-based stochastic model (GBSM) achieve greater accuracy by integrating simplified ray-tracing with statistical scatterer distributions. This combination enables a comprehensive framework for channel analysis, encompassing variations in multipath components (MPCs), spatial correlation, path clustering, directivity, and scatterer densification. GBSM analysis was employed in [23] to assess the impact of UAV rotation relative to the pitch axis, modeled with a deterministic periodic function. However, the authors constrained the placement of the UAV, user equipment (UE), and antennas, thus preventing the evaluation of the location of the antenna relative to the UAV platform on jitter, as well as hindering the reusability of these models for network channel prediction methods. In [24], random jittering/wobbling on the pitch axis is modeled as a Wiener and sinusoidal process, where the distance from the antenna to the centroid of the UAV is considered. In [25], jitter analysis in air-to-air communication is done similarly to [23] and [24]. Since the sources of disturbance are not only wind, but can also come from internal vibrations and instabilities, the authors in [26] propose to consider the effects of jitter on the three axes: pitch, roll and yaw. In [27], 3D jittering/wobbling is also considered, but with Gaussian distribution and LoS link, where beam training that reduces the impact of jitter is proposed for UAV mmWave communications. Finally, it is also worth highlighting the study in [28] on jittering/wobbling that takes into account the radial velocity component of the UAV.

C. Novelty and Contributions

The existing literature provides evidence of jitter as an important criterion for optimizing solutions for UAV communication. However, their models are simplified for study purposes and are not generalizable to wireless communication networks. Furthermore, the literature lacks methods for mitigating jitter, and, as far as we know, there are no CSI prediction solutions aimed at mitigating 3D jittering/wobbling along with the effect of conventional channel aging. Based on these studies, observations and background, we are motivated to analyze and mitigate the impact of 3D jittering/wobbling in air-to-ground wireless communications, focusing on addressing channel aging inherent to network-connected UAVs with space-time CSI Bayesian prediction, where general space-time correlation functions considering the jitter effect are necessary. The main related works with their characteristics and configurations are listed and compared with those of the present paper in Tab. I (at the top of next page).

This work addresses the following questions, which form the main contributions:

- How does jittering/wobbling imply channel aging? From the perspective of GBSM, variations in antenna attitude cause small-scale changes in path length, thereby affecting the phase of signal replicas. Since angular variations can lead to beam misalignment and phase shifts can alter the interference profile of MPCs, we demonstrate that random fluctuations in the UAV platform can have a significant impact on channel aging.
- Is it possible to model the channel using a steering vector while considering the effects of jittering/wobbling? The steering vector-based channel model offers advantages for analyzing and implementing channel estimators, precoders, or receivers, as it allows for the separation of the channel model into the antenna array model and the fading model. We demonstrate that this separation remains viable with GBSM.
- Does the placement of antennas on the UAV platform affect the impact of jittering/wobbling on the channel aging? We demonstrate that the further the antennas are positioned from the UAV centroid, the more pronounced the jitter becomes. This is attributed to the widening angular aperture of the UAV's swinging motion, leading to greater variations in path length.
- Can the integration of channel correlation function with jittering/wobbling into Bayesian channel predictor designs compensate, even partially, the effects of channel aging on spectral efficiency (SE)? The answer is yes. To demonstrate this, we develop general autocorrelation functions (ACFs) considering jitter and observe its impact on the downlink rate of single-user multi-stream communication between an access point (AP) and UAV, operating with mmWave bands, uniform planar array (UPA) and hybrid precoders under non-isotropic scattering conditions, typical of small cells and cell-free environment [29]. Next, we propose a directional CSI predictor based on extended Kalman filter (EKF) [30], P-order autoregressive (AR) process, or AR(P) and the ACFs determined to mitigate its impact. Then, we show, through numerical simulation, that the effect of fluctuations on the downlink data rate can be partially overcome using an EKF predictor.

This paper is structured as follows. Section II describes the proposed system model and theorems, the proofs of which

TABLE I: Summary of state of the art related to jittering analysis.

Reference	UAV Fluctuation Analysis	Mitigation	UAV Communication & Application	Architecture
Mohammad et al. [22]	– 3D hovering fluctuations – Gaussian deviation model – 3D LoS channel	Adjustment of antenna directivity gain	– UAV-assisted network – Point-to-point directive communication – BS-to-UAV – UAV-to-UAV	ULA mmWave
Zhangfeng et al. [23]	– 1D rotations – Nonrandom – Simplified 3D GBSM channel – Space-time-frequency CF	no	– Point-to-point directive communication – UAV-to-UE	ULA sub-6 Ghz
Morteza Banagar et al. [24]	– 1D wobbling – Wiener and sinusoidal process – Simplified 3D GBSM channel – Time ACF	no	– UAV-to-UE	Single antenna sub-6 Ghz
B. Yang and W. Zhang [25]	– 1D wobbling – Space-time CF – Simplified 3D GBSM channel	no	– UAV-to-UAV	ULA sub-6 Ghz
Xiaobo Yan et al. [26]	– 3D wobbling – Sinusoidal process – Simplified 3D GBSM channel – Time ACF	no	– UAV-to-UE	Single omni. Antenna sub-6 Ghz
W. Wang and W. Zhang [27]	– 3D wobbling – Gaussian deviation – 3D LoS channel	Beam training scheme Assisted by navigation Information	– BS-to-UAV – Point-to-point directive communication	UPA mmWave
Songiiang Yang et al. [28]	– 1D wobbling – Gaussian process – 3D LoS channel – Time ACF – Radial velocity	no	– BS-to-UAV	Single omni. Antenna mmWave
Present paper	– 3D wobbling – Wiener process – General 3D GBSM channel – Space-time CF	Channel prediction based on EKF-AR(P)	– Network-connected UAV – AP-to-UAV – Point-to-point MIMO – Channel aging	UPA mmWave

are presented in Appendices A and B. Section III explains in details the proposed predictor. Section IV presents the main numerical results and discussions. Finally, Section V summarizes the main insights and concludes our research.

$(\cdot)^{\dagger}$ and $(\cdot)^{\top}$ denote the Hermitian transpose and transpose of a matrix/vector, respectively. $|\cdot|$, $\|\cdot\|$ and $\|\cdot\|_{\mathrm{F}}$ the absolute value of a scalar, the norm of a vector and the Frobenius norm of a matrix, respectively. $[\mathbf{A}]_{n,m}$ and $[\boldsymbol{a}]_n$ denote the (n,m)-th element of the matrix $\mathbf{A}$ and (n)-th element of the vector $\boldsymbol{a}$, respectively. $f(\cdot)$ and $f[\cdot]$ denote continuous and discrete argument function, respectively. $\mathbb{E}[\cdot]$, $\mathrm{diag}(\cdot)$, $\langle\cdot\rangle$ and $\dot{x}$ denote the statistical expectation, diagonal of the matrix, inner product and first order derivative, respectively.

II. System Model

Let us consider a single user MIMO system, where the AP and UAV are equipped with a UPA of $N_{\mathrm{A}} = N_x \times N_y$ antenna elements and N_{RF} radio frequency (RF) chains in a fully-connected hybrid beamforming (HBF) architecture, with N_{S} streams multiplexing capability, such that $N_{\mathrm{S}} \leq N_{\mathrm{RF}} < N_{\mathrm{A}}$. The AP is connected to a central processing unit (CPU) via error-free fronthaul link [31]. We consider a single frame divided into τ_{S} time-slots. The communication is divided into two phases: uplink training and downlink data transmission [32]. The downlink channel is considered to be reciprocal to the uplink channel, an assumption that holds true in time division duplex (TDD) mode [33]. The system model is discrete and described as a function of the time-slot index n. We consider that a time-slot contains a resource block and that the channel aging delay is one time-slot. The duration of a time-slot is defined based on the symbol period T_{s}.

A. Space-Time Channel Model

A UPA is installed on the UAV platform at a relative distance from the UAV centroid, experiencing periodic fluctuations in attitude due to sources of adverse instability. Consider the local coordinate system (LCS) of the antenna elements transmitter (superscript T) with uniform spacing δ^{T}

$$\mathbf{A}'_{\mathbf{p}} = \begin{bmatrix} 0.5\delta^{\mathrm{T}}\left(N_x^{\mathrm{T}} - 2p_x + 1\right) \\ 0.5\delta^{\mathrm{T}}\left(N_y^{\mathrm{T}} - 2p_y + 1\right) \\ 0 \end{bmatrix} \tag{1}$$

and of the receive antenna elements (superscript R) with uniform spacing δ^{R}

$$\mathbf{A}'_{\mathbf{q}} = \begin{bmatrix} 0.5\delta^{\mathrm{R}}\left(N_x^{\mathrm{R}} - 2q_x + 1\right) \\ 0.5\delta^{\mathrm{R}}\left(N_y^{\mathrm{R}} - 2q_y + 1\right) \\ 0 \end{bmatrix} - \mathbf{C}^{\mathrm{UAV}\prime}\ , \tag{2}$$

where $\mathbf{C}^{\mathrm{UAV}\prime} = [c_x, c_y, c_z]^{\top}$ is the relative position of the centroid of the UAV platform. Assume that the UPAs are mounted in the xy-plane. We define the global coordinate system (GCS) with respect to the origin O as:

$$\mathbf{A}_{\mathbf{p}} = \mathbf{R}(0)\mathbf{A}'_{\mathbf{p}} \tag{3}$$

and

$$\mathbf{A}_{\mathbf{q}}(t) = \mathbf{R}(t)\mathbf{A}'_{\mathbf{q}}\ , \tag{4}$$

where $\mathbf{R}$ is the global rotation matrix defined in (5) (top of the next page), $\Psi_X \in [-\pi, \pi]$, $\Psi_Y \in [-\pi/2, \pi/2]$ and

$\Psi_Z \in [-\pi, \pi]$ represent the *roll*, *pitch* and *yaw* rotation angles, respectively. Here we represent the indices of the antenna element of a UPA by vectors $\mathbf{p} = [p_x, p_y]$ and $\mathbf{q} = [q_x, q_y]$, and we map each vector to a scalar, such as $p \to \mathbf{p}$ and $q \to \mathbf{q}$, when convenient.

We adopt spherical coordinates in the convention where $\phi \in [-\pi, \pi]$ (azimuth) and $\theta \in [-\pi/2, \pi/2]$ (elevation). AP and UAV locations are represented in relation to the global origin by distance vectors $\mathbf{D}^{\mathrm{AP}}$ and $\mathbf{D}^{\mathrm{UAV}}$, respectively. We assume that the transmission is from the AP to the UAV, and the LoS angles are determined with respect to the transmitter. We also define the following types of distance vectors: from the transmitter T to the scatterers cluster S, denoted by $\mathbf{D}^{\mathrm{TS}}$; from the receiver T to the scatterers cluster S, denoted by $\mathbf{D}^{\mathrm{RS}}$; and from the transmitter T to the receiver R, denoted by $\mathbf{D}^{\mathrm{LoS}}$. Likewise, we add the subscript ls to the distance vectors $\mathbf{D}^{\mathrm{TS}}$ and $\mathbf{D}^{\mathrm{RS}}$ to denote the s-th intra-path of the l-th cluster. The mobility of the UAV is represented by the velocity vector $\mathbf{v}^{\mathrm{UAV}}$. Lastly, we define the unit propagation vector as follows:

$$\boldsymbol{k}(\phi, \theta) \coloneqq \frac{\mathbf{D}}{\|\mathbf{D}\|_2} = \begin{bmatrix} \cos\phi\cos\theta \\ \sin\phi\cos\theta \\ \sin\theta \end{bmatrix} , \tag{6}$$

where $\mathbf{D}$ is an arbitrary distance vector. The superscripts AP, UAV, LoS, TS and RS are used in the other channel path parameters for the same definitional purpose.

Simplified channel models based on steering vectors are prevalent in the literature [34]. These models provide a framework for designing channel estimators and minimum mean square error (MMSE) receivers. Consequently, it is crucial to assess the applicability of such models in the context of air-to-ground wireless channels, accounting for the effects of UAV platform fluctuations and their potential impact on the correction function. To this end, we introduce the following theorems (our model was inspired by 3D-GBSM papers [35], [36], [37], [38]):

Theorem 1. *The air-to-ground channel response, single-bounced at the Tx side (SBT), with antenna attitude fluctuations can be approximately expressed in terms of complex gain and steering vector:*

$$\mathbf{H}_{ls}^{\mathrm{SBT}}(t) \approx g_{ls}^{\mathrm{SBT}}(t)\mathbf{a}_{\mathrm{UAV}}\left(\phi_{ls}^{\mathrm{RS}}, \theta_{ls}^{\mathrm{RS}}, t\right)\mathbf{a}_{\mathrm{AP}}^{\dagger}\left(\phi_{ls}^{\mathrm{TS}}, \theta_{ls}^{\mathrm{TS}}\right) , \tag{7}$$

where

$$H_{pq,ls}^{\mathrm{SBT}}(t) \approx g_{ls}^{\mathrm{SBT}}(t)\mathrm{a}_q\left(\phi_{ls}^{\mathrm{RS}}, \theta_{ls}^{\mathrm{RS}}, t\right)\mathrm{a}_p^{*}\left(\phi_{ls}^{\mathrm{TS}}, \theta_{ls}^{\mathrm{TS}}\right) , \tag{8}$$

such that the non-line of sight (NLoS) complex gain is

$$\begin{aligned} g_{ls}^{\mathrm{SBT}}(t) = \sqrt{\eta_{ls}^{\mathrm{SBT}}}\exp\left\{-\mathrm{j}\,\frac{2\pi}{\lambda}\left(\|\mathbf{D}_{ls}^{\mathrm{TS}}\|_2 + \|\mathbf{D}_{ls}^{\mathrm{RS}}\|_2\right)\right\} \\ \times \exp\left\{\mathrm{j}\,\frac{2\pi}{\lambda}t f_{\mathrm{d},ls}^{\mathrm{SBT}}\right\} \end{aligned} \tag{9}$$

and spatial signature is

$$\mathbf{a}(\phi, \theta, t) = \frac{1}{\sqrt{N_{\mathrm{A}}}}\left[\mathrm{a}_1(\phi, \theta, t), \mathrm{a}_2(\phi, \theta, t), \ldots, \mathrm{a}_{N_{\mathrm{A}}}(\phi, \theta, t)\right]^{\top} , \tag{10}$$

with

$$\mathrm{a}_{p(q)}(\phi, \theta, t) = \exp\left(-\mathrm{j}\,\frac{2\pi}{\lambda}\mathbf{A}_{\mathbf{p}(\mathbf{q})}(t)^{\top}\boldsymbol{k}(\phi, \theta)\right) . \tag{11}$$

Proof. The proofs are developed in Appendix A. □

Corollary 1. *The LoS air-to-ground channel response with antenna attitude fluctuations can be approximately expressed in terms of complex gain and steering vector:*

$$\mathbf{H}^{\mathrm{LoS}}(t) \approx g^{\mathrm{LoS}}(t)\mathbf{a}_{\mathrm{UAV}}\left(\phi^{\mathrm{LoS}}, \theta^{\mathrm{LoS}}, t\right)\mathbf{a}_{\mathrm{AP}}^{\dagger}\left(\phi^{\mathrm{LoS}}, \theta^{\mathrm{LoS}}\right) , \tag{12}$$

such that the complex gain of the channel is

$$g^{\mathrm{LoS}}(t) = \sqrt{\eta^{\mathrm{LoS}}}\exp\left\{-\mathrm{j}\,\frac{2\pi}{\lambda}\|\mathbf{D}^{\mathrm{LoS}}\|_2\right\}\exp\left\{\mathrm{j}\,\frac{2\pi}{\lambda}t f_{\mathrm{d}}^{\mathrm{LoS}}\right\} .$$

where $f_{\mathrm{d}}^{\mathrm{LoS}} = \langle \boldsymbol{k}^{\mathrm{LoS}}, \mathbf{v}^{\mathrm{UAV}} \rangle$ *and* $\mathbf{D}^{\mathrm{LoS}} = \mathbf{D}^{\mathrm{UAV}} - \mathbf{D}^{\mathrm{AP}}$.

B. UAV Platform Fluctuations

Assumption 1. *Changes in the elevation (roll), orientation (yaw) and inclination (pitch) of the UAV array antennas occur due to engine vibration and turbulence occur periodically.*

Consider that Ψ is any of the three angles: Ψ_Z (yaw), Ψ_Y (pitch) and Ψ_X (roll). The UAV platform fluctuations can be modeled by a sinusoidal process with amplitude A_Ψ and frequency F_Ψ, such that:

$$\Psi(t) = \Psi(0) + A_\Psi \sin(2\pi F_\Psi t) . \tag{13}$$

Parameters A_Ψ and F_Ψ can be deterministic [23] or random [26] in relation to time. The linear approximation for a time-shift Δt around an arbitrary w-axis is:

$$\begin{aligned} \cos\left(\Psi(t+\Delta t)\right) &\approx \cos\Psi(t) - \sin\Psi(t)\dot{\Psi}(t)\Delta\Psi_{\Delta t} , \\ \sin\left(\Psi(t+\Delta t)\right) &\approx \sin\Psi(t) + \cos\Psi(t)\dot{\Psi}(t)\Delta\Psi_{\Delta t} , \end{aligned} \tag{14}$$

then

$$\begin{aligned} \mathbf{R}_W(t+\Delta t) &= \begin{bmatrix} +\cos\Psi(t+\Delta t) & 0 & +\sin\Psi(t+\Delta t) \\ 0 & 1 & 0 \\ -\sin\Psi(t+\Delta t) & 0 & +\cos\Psi(t+\Delta t) \end{bmatrix} \\ &\approx \begin{bmatrix} +\cos\Psi(t) & 0 & +\sin\Psi(t) \\ 0 & 1 & 0 \\ -\sin\Psi(t) & 0 & +\cos\Psi(t) \end{bmatrix} \\ &\quad + \begin{bmatrix} -\sin\Psi(t) & 0 & +\cos\Psi(t) \\ 0 & 0 & 0 \\ -\cos\Psi(t) & 0 & -\sin\Psi(t) \end{bmatrix}\dot{\Psi}(t)\Delta\Psi_{\Delta t} \\ &= \mathbf{R}_W(t) + \dot{\mathbf{R}}_W(t)\Delta\Psi_{\Delta t} , \end{aligned} \tag{15}$$

where

$$\mathbf{R}_W(t) = \begin{bmatrix} +\cos\Psi(t) & 0 & +\sin\Psi(t) \\ 0 & 1 & 0 \\ -\sin\Psi(t) & 0 & +\cos\Psi(t) \end{bmatrix}$$

and

$$\dot{\mathbf{R}}_W(t) = \begin{bmatrix} -\sin\Psi(t) & 0 & +\cos\Psi(t) \\ 0 & 0 & 0 \\ -\cos\Psi(t) & 0 & -\sin\Psi(t) \end{bmatrix}\dot{\Psi}(t) .$$

$$\begin{aligned}\mathbf{R}(t) &= \mathbf{R}_Z(t)\mathbf{R}_Y(t)\mathbf{R}_X(t) \\ &= \begin{bmatrix} +\cos\Psi_Z(t) & -\sin\Psi_Z(t) & 0 \\ +\sin\Psi_Z(t) & +\cos\Psi_Z(t) & 0 \\ 0 & 0 & 1 \end{bmatrix} \begin{bmatrix} +\cos\Psi_Y(t) & 0 & +\sin\Psi_Y(t) \\ 0 & 1 & 0 \\ -\sin\Psi_Y(t) & 0 & \cos\Psi_Y(t) \end{bmatrix} \begin{bmatrix} 1 & 0 & 0 \\ 0 & +\cos\Psi_X(t) & -\sin\Psi_X(t) \\ 0 & +\sin\Psi_X(t) & +\cos\Psi_X(t) \end{bmatrix} .\end{aligned} \tag{5}$$

For sinusoidal processes as in (13), it follows that:

$$\dot{\Psi}(t) = 2\pi A_\Psi F_\Psi \cos(2\pi F_\Psi t) \text{ and } \Delta\Psi_{\Delta t} = \Delta t \ .$$

Assuming that A_Ψ and F_Ψ are random, the matrices $\dot{\mathbf{R}}_X(t)$, $\dot{\mathbf{R}}_Y(t)$ and $\dot{\mathbf{R}}_Z(t)$ are also random. Considering that $\Delta\Psi_{\Delta t}$ is very small and therefore $\Delta\Psi^2_{\Delta t} \approx \Delta\Psi^3_{\Delta t} \approx 0$, we can extend it to a 3D model:

$$\begin{aligned}\mathbf{R}(t+\Delta t) &= \mathbf{R}_Z(t+\Delta t)\mathbf{R}_Y(t+\Delta t)\mathbf{R}_X(t+\Delta t) \\ &\approx \mathbf{R}(t) + \dot{\mathbf{R}}(t)\Delta\Psi_{\Delta t} \ ,\end{aligned} \tag{16}$$

where

$$\begin{aligned}\dot{\mathbf{R}}(t) &= \dot{\mathbf{R}}_Z(t)\mathbf{R}_Y(t)\mathbf{R}_X(t) + \mathbf{R}_Z(t)\dot{\mathbf{R}}_Y(t)\mathbf{R}_X(t) \\ &\quad + \mathbf{R}_Z(t)\mathbf{R}_Y(t)\dot{\mathbf{R}}_X(t) \ .\end{aligned}$$

Note that the $\dot{\mathbf{R}}(t)$ matrix contains the jitter in the three axes, each of which can have different amplitudes and frequencies, as also indicated in (5).

C. Autocorrelation Function

To comprehend how fluctuations in antenna attitude may influence the channel coherence time, and consequently, the extent of channel aging, we formulate the following theorem concerning the time ACF.

Theorem 2. *The time ACF of an intra-cluster air-to-ground channel of the SBT type with UAV platform fluctuations can be approximated by:*

$$\begin{aligned}\mathrm{ACF}_l(t,\mathbf{q};\Delta t) \approx \eta_l^{\mathrm{SBT}} \mathbb{E}\Bigg[&\exp\Big\{ \mathrm{j}\,\frac{2\pi}{\lambda}\Delta t \langle \boldsymbol{k}_{ls}^{\mathrm{RS}}, \mathbf{v}^{\mathrm{UAV}} \rangle \Big\} \\ &\times \exp\Big\{ -\mathrm{j}\,\frac{2\pi}{\lambda}\Delta\Psi_{\Delta t} \mathbf{A}_{\mathbf{q}}'^{\top} \dot{\mathbf{R}}^{\top}(t) \boldsymbol{k}_{ls}^{\mathrm{RS}} \Big\} \Bigg] \ ,\end{aligned} \tag{17}$$

where the expectation is related to the distribution of scatterers and UAV fluctuations.

Proof. The proofs are developed in Appendix B. □

Considering the assumption that the LoS component is deterministic and thus its wave vector $\boldsymbol{k}^{\mathrm{LoS}}$ is a non-random variable, the following corollary arises:

Corollary 2. *The time ACF of an LoS air-to-ground channel with UAV platform fluctuations can be approximated by:*

$$\begin{aligned}\mathrm{ACF}(t,\mathbf{q};\Delta t) \approx &\eta^{\mathrm{LoS}} \exp\Big\{ \mathrm{j}\,\frac{2\pi}{\lambda}\Delta t \langle \boldsymbol{k}^{\mathrm{LoS}}, \mathbf{v}^{\mathrm{UAV}} \rangle \Big\} \\ &\times \mathbb{E}\Bigg[\exp\Big\{ -\mathrm{j}\,\frac{2\pi}{\lambda}\Delta\Psi_{\Delta t} \mathbf{A}_{\mathbf{q}}'^{\top} \dot{\mathbf{R}}^{\top}(t) \boldsymbol{k}^{\mathrm{LoS}} \Big\} \Bigg] \ ,\end{aligned} \tag{18}$$

where the expectation is related to the UAV fluctuations.

Consider the relative coordinates of the antennas in (2). Replacing $\mathbf{A}_{\mathbf{q}}'$ within (17), we have the following expectation:

$$\begin{aligned}&\mathbb{E}\Bigg[\exp\Big\{ -\mathrm{j}\,\frac{2\pi}{\lambda}\Delta\Psi_{\Delta t} \mathbf{A}_{\mathbf{q}}'^{\top} \dot{\mathbf{R}}^{\top}(t) \boldsymbol{k}_{ls}^{\mathrm{RS}} \Big\} \Bigg] \\ &= \mathbb{E}\Bigg[\exp\Big\{ -\mathrm{j}\,\frac{2\pi}{\lambda}\Delta\Psi_{\Delta t} \begin{bmatrix} 0.5\delta^{\mathrm{R}}\left(N_x^{\mathrm{R}} - 2q_x + 1\right) \\ 0.5\delta^{\mathrm{R}}\left(N_y^{\mathrm{R}} - 2q_y + 1\right) \\ 0 \end{bmatrix}^{\top} \dot{\mathbf{R}}^{\top}(t) \boldsymbol{k}_{ls}^{\mathrm{RS}} \Big\} \\ &\times \exp\Big\{ \mathrm{j}\,\frac{2\pi}{\lambda}\Delta\Psi_{\Delta t} \mathbf{C}^{\mathrm{UAV}\prime\top} \dot{\mathbf{R}}^{\top}(t) \boldsymbol{k}_{ls}^{\mathrm{RS}} \Big\} \Bigg] \ ,\end{aligned}$$

where it is observed that the distance $\mathbf{C}^{\mathrm{UAV}\prime}$ influences the phase of the signal replicas and, consequently, the ACF. The same applies to the LoS component. Therefore, we define the following corollary:

Corollary 3. *The location of the UAV antenna $\mathbf{A}_{\mathbf{q}}'$ (2) influences the air-to-ground channel ACF with UAV platform fluctuations.*

III. EKF-BASED PREDICTOR

Channel prediction can be approximated using parametric functions and correlation functions. The model incorporates channel correlations with jitter through AR processes. This approximation enables the implementation of parametric channel estimators and reduces training overhead [39], [40]. For small antenna arrays, we neglect the correlation difference between MIMO subchannels, as demonstrated in the Theorem 1. This is achieved by separating temporal correlation from spatial correlation. In this way, temporal correlation can be generated using one-dimensional AR models based on Theorem 2 without the need for cross-correlation, making it more practical. Therefore, in this section, we propose a Bayesian predictor of directional CSI based on EKF and AR(P) that takes into account the ACF of the channel with jitter. Using this directional CSI predictor, it is possible to mitigate the effects of channel aging due to jittering/wobbling and Doppler shift.

A. Propagation Parameter Transition Model

Consider a time-slot delay between the moment when the channel is estimated and the moment when the precoder is applied. Assuming that the ACF is known and given by Theorem 2, the small-scale gain for each independent dominant

path[1] l at the n-th time-slot can be estimated by

$$\widehat{\alpha}_l[n] = \sum_{p=1}^{P} a_{l,p}\widehat{\alpha}_l[n-p] + u_{\widehat{\alpha}}[n] \ , \tag{19}$$

where P is the filter order, $a_{l,p} \in \mathbb{C}$ are the filter coefficients and $u_{\widehat{\alpha}} \sim \mathcal{CN}(0, \sigma^2_{\widehat{\alpha},l})$ is a circular complex white Gaussian noise (with uncorrelated real and imaginary components). The coefficients $a_{l,p}$ are determined via the Yule-Walker equations [41].

The stochastic model for the azimuth ϕ and elevation θ components of the angle of arrival (AoA) (subscript A) and angle of departure (AoD) (subscript D) at the n-th time-slot are represented by a Gaussian random walk [42]:

$$\begin{aligned} \widehat{\theta}_{\mathrm{A(D)},l}[n] &= \widehat{\theta}_{\mathrm{A(D)},l}[n-1] + u_{\theta_{\mathrm{A(D)}}}[n] \ , \\ \widehat{\phi}_{\mathrm{A(D)},l}[n] &= \widehat{\phi}_{\mathrm{A(D)},l}[n-1] + u_{\phi_{\mathrm{A(D)}}}[n] \ , \end{aligned} \tag{20}$$

where $u_{\theta_{\mathrm{A(D)}}} \sim \mathcal{N}(0, \sigma^2_\theta)$ and $u_{\phi_{\mathrm{A(D)}}} \sim \mathcal{N}(0, \sigma^2_\phi)$, so that σ^2_θ and σ^2_ϕ control the angular temporal variation. In this paper, we assume that these angular variations are sufficiently small to not influence the ACF. This assumption holds true for short periods of time.

B. EKF State Model

Consider the following variables in the time-slot n: $\boldsymbol{\theta}_{\mathrm{D}}[n] = \left[\widehat{\theta}_{\mathrm{D},1}[n], \ldots, \widehat{\theta}_{\mathrm{D},L}[n]\right]$, $\boldsymbol{\theta}_{\mathrm{A}}[n] = \left[\widehat{\theta}_{\mathrm{A},1}[n], \ldots, \widehat{\theta}_{\mathrm{A},L}[n]\right]$, $\boldsymbol{\phi}_{\mathrm{D}}[n] = \left[\widehat{\phi}_{\mathrm{D},1}[n], \ldots, \widehat{\phi}_{\mathrm{D},L}[n]\right]$, $\boldsymbol{\phi}_{\mathrm{A}}[n] = \left[\widehat{\phi}_{\mathrm{A},1}[n], \ldots, \widehat{\phi}_{\mathrm{A},L}[n]\right]$, $\boldsymbol{\alpha}_{\mathrm{Re}}[n] = \Re\left(\left[\widehat{\alpha}_1[n], \ldots, \widehat{\alpha}_L[n]\right]\right)$ and $\boldsymbol{\alpha}_{\mathrm{Im}}[n] = \Im\left(\left[\widehat{\alpha}_1[n], \ldots, \widehat{\alpha}_L[n]\right]\right)$, where $\Re(\cdot)$ and $\Im(\cdot)$ are the real and imaginary components, respectively. We define the state vector $\overline{\boldsymbol{x}}[n]$ of order P as:

$$\overline{\boldsymbol{x}}[n] = \left[\boldsymbol{\phi}_{\mathrm{A}}[n], \boldsymbol{\phi}_{\mathrm{D}}[n], \boldsymbol{\theta}_{\mathrm{A}}[n], \boldsymbol{\theta}_{\mathrm{D}}[n], \overline{\boldsymbol{\alpha}}[n]\right]^\top \quad \in \mathbb{R}^{D_{\overline{\mathrm{x}}} \times 1} \ , \tag{21}$$

where

$$\overline{\boldsymbol{\alpha}}[n] = \left[\boldsymbol{\alpha}[n], \boldsymbol{\alpha}[n-1], \cdots, \boldsymbol{\alpha}[n-P+1]\right]^\top \in \mathbb{R}^{2LP \times 1},$$

and

$$\boldsymbol{\alpha}[n] = \left[\boldsymbol{\alpha}_{\mathrm{Re}}[n], \boldsymbol{\alpha}_{\mathrm{Im}}[n]\right]^\top \quad \in \mathbb{R}^{2L \times 1} \ ,$$

such that $\overline{\boldsymbol{x}}[n]$ has dimension $D_{\overline{\mathrm{x}}} = 4L + 2LP$. Given a channel time evolution model defined by (19) and (20), the EKF state transition equation is given by:

$$\overline{\boldsymbol{x}}[n+1] = \overline{\mathbf{A}}\overline{\boldsymbol{x}}[n] + \boldsymbol{u}_{\overline{\mathrm{x}}}[n+1] \ , \tag{22}$$

where $\overline{\boldsymbol{x}}[n+1]$ is the *a posteriori* prediction and $\overline{\mathbf{A}}$ is the state transition matrix given by:

$$\overline{\mathbf{A}} = \begin{bmatrix} \mathbf{A}_1 & \mathbf{0}_{4L \times 2LP} \\ \mathbf{0}_{2LP \times 4L} & \mathbf{A}_2 \end{bmatrix} \quad \in \mathbb{R}^{D_{\overline{\mathrm{x}}} \times D_{\overline{\mathrm{x}}}} \ , \tag{23}$$

[1]The term "dominant paths" is commonly used in the mmWave channel models due to its sparse nature. Although the literature does not explicitly define the origin of these paths, it often considers those with greater gain as dominant. For instance, these dominant paths could encompass the LoS, a signal reflected from the ground, or a cluster. If the cluster originates from a local dispersion, it can be perceived as a single path by the receiver, as the delays, AoAs, AoDs, and Doppler frequencies of its intra-paths are very close, which can be represented by the average of its intra-paths, for example.

such that

$$\mathbf{A}_1 = \mathbf{I}_{4L} \quad \in \mathbb{R}^{4L \times 4L} \ ,$$

$$\mathbf{A}_2 = \begin{bmatrix} \overline{\mathbf{A}}_{2,1} & \overline{\mathbf{A}}_{2,2} & \cdots & \overline{\mathbf{A}}_{2,P-1} & \overline{\mathbf{A}}_{2,P} \\ \mathbf{I}_{2L} & \mathbf{0}_{2L} & \cdots & \mathbf{0}_{2L} & \mathbf{0}_{2L} \\ \mathbf{0}_{2L} & \mathbf{I}_{2L} & \cdots & \mathbf{0}_{2L} & \mathbf{0}_{2L} \\ \vdots & \vdots & \ddots & \vdots & \vdots \\ \mathbf{0}_{2L} & \mathbf{0}_{2L} & \cdots & \mathbf{I}_{2L} & \mathbf{0}_{2L} \end{bmatrix} \in \mathbb{R}^{2LP \times 2LP} \ ,$$

and

$$\overline{\mathbf{A}}_{2,p} = \begin{bmatrix} \Re\left(\mathbf{A}_{2,p}\right) & -\Im\left(\mathbf{A}_{2,p}\right) \\ \Im\left(\mathbf{A}_{2,p}\right) & \Re\left(\mathbf{A}_{2,p}\right) \end{bmatrix} \quad \in \mathbb{R}^{2L \times 2L} \ ,$$

where $\mathbf{A}_{2,p} \in \mathbb{C}^{L \times L}$ is the coefficient matrix of the channel generator AR filter. For uncorrelated channels, it follows that $\mathbf{A}_{2,p} = \mathrm{diag}\left(\boldsymbol{a}_p\right) = \mathrm{diag}\left(\left[a_{1,p}, \cdots, a_{L,p}\right]\right)$. The vector $\boldsymbol{u}_{\overline{\mathrm{x}}}$ is the innovation process given by:

$$\boldsymbol{u}_{\overline{\mathrm{x}}}[n] \sim \mathcal{N}(\mathbf{0}, \mathbf{Q}_{\mathrm{u}_{\overline{\mathrm{x}}}\mathrm{u}_{\overline{\mathrm{x}}}}) \in \mathbb{R}^{D_{\overline{\mathrm{x}}} \times 1} \ , \tag{24}$$

such that

$$\mathbf{Q}_{\mathrm{u}_{\overline{\mathrm{x}}}\mathrm{u}_{\overline{\mathrm{x}}}} = \overline{\mathbf{B}}\mathbf{Q}_{\mathrm{u}_{\mathrm{x}}\mathrm{u}_{\mathrm{x}}}\overline{\mathbf{B}}^\top \quad \in \mathbb{R}^{D_{\overline{\mathrm{x}}} \times D_{\overline{\mathrm{x}}}} \ ,$$

where $\mathbf{Q}_{\mathrm{u}_{\mathrm{x}}\mathrm{u}_{\mathrm{x}}}$ is the covariance matrix of the process noise to the state vector

$$\widehat{\boldsymbol{x}}[n] = \left[\boldsymbol{\phi}_{\mathrm{A}}[n], \boldsymbol{\phi}_{\mathrm{D}}[n], \boldsymbol{\theta}_{\mathrm{A}}[n], \boldsymbol{\theta}_{\mathrm{D}}[n], \boldsymbol{\alpha}[n]\right]^\top \quad \in \mathbb{R}^{6L \times 1},$$

and

$$\overline{\mathbf{B}} = \left[\mathbf{I}_{6L}, \mathbf{0}_{6L}, \cdots, \mathbf{0}_{6L}\right]^\top \quad \in \mathbb{R}^{D_{\overline{\mathrm{x}}} \times 6L} \ .$$

C. EKF Observation Model

It is possible to train up to N^2_{RF} beam pairs simultaneously per symbol. Consider an RF beamforming codebook $\mathcal{B}$ of size $B = |\mathcal{B}|$. If the training beamsets $\mathbf{F}_{\mathrm{RF}} \in \mathbb{C}^{N_{\mathrm{A}} \times B_{\mathrm{F}}}$ and $\mathbf{W}_{\mathrm{RF}} \in \mathbb{C}^{N_{\mathrm{A}} \times B_{\mathrm{W}}}$, such that $[\mathbf{F}_{\mathrm{RF}}]_{:,i} \subseteq \mathcal{B}$, $[\mathbf{W}_{\mathrm{RF}}]_{:,j} \subseteq \mathcal{B}$, $B_{\mathrm{F}} \leq B$ and $B_{\mathrm{W}} \leq B$, are used for transmission and reception respectively, the sets can be divided into $N_{\mathrm{F}} = \lceil \frac{B_{\mathrm{F}}}{N_{\mathrm{RF}}} \rceil$ and $N_{\mathrm{W}} = \lceil \frac{B_{\mathrm{W}}}{N_{\mathrm{RF}}} \rceil$ unique parts, like $\mathbf{F}_{\mathrm{RF}} = [\mathbf{F}_{\mathrm{RF},1}, \cdots, \mathbf{F}_{\mathrm{RF},N_{\mathrm{F}}}]$ and $\mathbf{W}_{\mathrm{RF}} = [\mathbf{W}_{\mathrm{RF},1}, \cdots, \mathbf{W}_{\mathrm{RF},N_{\mathrm{W}}}]$, then $\tau_{\mathrm{p}} = N_{\mathrm{F}}N_{\mathrm{W}}$ pilot symbols are allocated inside each time-slot. The collection of all received beamforming pilots is given by:

$$\mathbf{Y}[n] = \sqrt{\varrho_{\mathrm{p}}}\mathbf{F}^\dagger_{\mathrm{RF}}\mathbf{H}_{\mathrm{UL}}[n]\mathbf{W}_{\mathrm{RF}} + \mathbf{U}_{\mathrm{UL}} \quad \in \mathbb{C}^{B_{\mathrm{F}} \times B_{\mathrm{W}}} \ , \tag{25}$$

where ϱ_{p} is the uplink effective power and $\mathbf{U}_{\mathrm{UL}}$ is the noise matrix with noise power σ^2_{UL} [40].

Building upon Theorems 1 and 2, our parametric model for estimating the channel of a path l within a specific quasi-stationary interval [23] starting at t is given by:

$$\widehat{\mathbf{H}}_{\mathrm{UL},l}[n] = \beta_l\widehat{\alpha}_l[n]\mathbf{a}_{\mathrm{AP}}\left(\widehat{\phi}_{\mathrm{A},l}, \widehat{\theta}_{\mathrm{A},l}, t\right)\mathbf{a}^\dagger_{\mathrm{UAV}}\left(\widehat{\phi}_{\mathrm{D},l}, \widehat{\theta}_{\mathrm{D},l}\right) \ , \tag{26}$$

where $\widehat{\mathbf{H}}_{\mathrm{UL}}$ is calculated with the backpropagated predicted state variable from the EKF as its argument, β_l is the time-invariant total gain and n is the time-slot starting at time t.

The non-linear observation model based on beamsearch training is given by:

$$\widehat{\mathbf{Y}}[n] = \mathbf{F}_{\mathrm{RF}}^{\dagger}\widehat{\mathbf{H}}_{\mathrm{UL}}[n]\mathbf{W}_{\mathrm{RF}} \quad \in \mathbb{C}^{B_{\mathrm{F}}\times B_{\mathrm{W}}} \ . \tag{27}$$

However, it is necessary to linearize the observation model (27) for EKF implementation. A linear approximation is made by calculating the Jacobian matrix $\mathbf{C}[n] \in \mathbb{C}^{D_{\overline{\mathrm{y}}}\times 6L}$ of $\widehat{\mathbf{Y}}[n]$, so that:

$$\mathbf{C}[n] = [c_{i,j}(\widehat{\boldsymbol{x}}[n])]_{1\leq i\leq D_{\overline{\mathrm{y}}},\ 1\leq j\leq 6L} \ , \tag{28}$$

with

$$c_{i,j}(\widehat{\boldsymbol{x}}[n]) = \frac{\partial \widehat{y}_i(\widehat{\boldsymbol{x}}[n])}{\partial \widehat{x}_j} \ , \tag{29}$$

where $\widehat{y}_i(\widehat{\boldsymbol{x}}[n])$ is an element of the matrix function $\widehat{\mathbf{Y}}[n]$, $D_{\overline{\mathrm{y}}} = B_{\mathrm{F}}B_{\mathrm{W}}$ and i the linear index.

D. EKF Gain

The EKF gain $\overline{\mathbf{K}} \in \mathbb{R}^{D_{\overline{\mathrm{x}}}\times D_{\overline{\mathrm{y}}}}$ is given by:

$$\overline{\mathbf{K}}[n] = \overline{\mathbf{P}}[n]\mathbf{C}^{\top}[n]\left(\mathbf{C}[n]\overline{\mathbf{P}}[n]\mathbf{C}^{\top}[n] + \mathbf{Q}_{\mathrm{u}_{\overline{\mathrm{y}}}\mathrm{u}_{\overline{\mathrm{y}}}}\right)^{-1} \ , \tag{30}$$

where $\overline{\mathbf{P}} \in \mathbb{R}^{D_{\overline{\mathrm{x}}}\times D_{\overline{\mathrm{x}}}}$ is the covariance matrix of the *a posteriori* prediction error of the state variable $\overline{\boldsymbol{x}}$, which is initialized based on ACF knowledge, and $\mathbf{Q}_{\mathrm{u}_{\overline{\mathrm{y}}}\mathrm{u}_{\overline{\mathrm{y}}}} \in \mathbb{R}^{D_{\overline{\mathrm{y}}}\times D_{\overline{\mathrm{y}}}}$ is the covariance matrix of the measurement noise.

E. Prediction

We assume a channel aging model as in [10], so that the CSI ages continuously every unit of time, and there is a delay, inherent to the network, between the training block and the data transmission block. This delay, influenced by propagation and processing time, represents the time needed for each transmitter in the network to update its precoder and begin data transmission. It is more pronounced in ultra-dense networks with coherent transmission [11], such as cell-free networks [29], operating in mmWave band [9]. Then, the channel is forecasted for one time-slot into the future, enabling the design of the corresponding precoder without aging based on the predicted channel. For this purpose, EKF is configured in prediction mode, so that the filter output corresponds to the parameters in the time-slot $n+1$.

F. Order of Complexity

Following the concept of asymptotic complexity, the computational cost of the problem treated with the EKF lies in the inversion of the filter gain matrix:

$$\left(\mathbf{C}[n]\overline{\mathbf{P}}[n]\mathbf{C}^{\top}[n] + \mathbf{Q}_{\mathrm{u}_{\overline{\mathrm{y}}}\mathrm{u}_{\overline{\mathrm{y}}}}\right)^{-1} \ ,$$

where its dimension $D_{\overline{\mathrm{y}}} \times D_{\overline{\mathrm{y}}}$ depends on the number of spatial measurements of the channel B_{F} and B_{W} throughout training. Therefore, the asymptotic computational complexity of the EKF, determined based on the matrix inversion operation, number of arithmetic operations and Gauss—Jordan elimination, is $\mathcal{O}\left(D_{\overline{\mathrm{y}}}^3\right)$.

IV. Numerical Results

In this section, we numerically evaluate the impact of UAV platform fluctuations on the ACF, specifically 3D jittering, and demonstrate the benefits of an EKF-based channel predictor on downlink rate. We evaluate the influence of wavelength, distance from the centroid, and jitter amplitude on the ACF. To calculate the correlation functions (17) and (34), we adopted random jitters, whose probability density functions (PDFs) are: $A_{\Psi} \sim \mathcal{U}(-\sigma_A, \sigma_A)$ and $F_{\Psi} \sim \mathcal{U}(F_1, F_2)$, with σ_A representing the maximum amplitude [24], [26]. For simplicity, we assume that jittering occurs with the same intensity in all three axes. The standard simulation setup is presented in Tab. II.

TABLE II: Default simulation setup.

Type	Parameter
Numerology [43]	$f_{\mathrm{c}} = 28.0$ GHz (FR2), Bandwidth $= 200.0$ MHz, $T_{\mathrm{s}} = 8.335 + 0.59 = 8.925$ μs, slot $= 14$ symb., $\tau_{\mathrm{S}} = 80$ slots, delay $= 1$ slot.
Channel [44], [45], [46]	$K_{\mathrm{R}} = 0$ (*NLoS scenario*), $L = 4$, Path Loss $= 120.0$ dB $\sigma_{\phi} = \sigma_{\theta} = 0.005°$, $N_{\mathrm{S}} = 2$, $\kappa_{\mathrm{AP}} = 3$, $\theta_{\mathrm{m,AP}} = \pi/4$, $R_{\mathrm{AP}} = 30.0$ m, $N_{\mathrm{A}} = 16$, $N_{\mathrm{RF}} = 8$, Ideal array total gain $= 24.0$ dB, Noise power spectral density $N_0 = -173.8$ dBm, Noise figure $= 7.0$ dB, Downlink data effective power $\varrho_{\mathrm{d}} = 17.1$ dB.
Positioning [23], [26], [24]	$\mathbf{D}^{\mathrm{AP}} = [0, 0, 15.0]^{\top}$, $\mathbf{D}^{\mathrm{UAV}} = [0, 0, 50.0]^{\top}$, $\mathbf{v}^{\mathrm{UAV}} = [0, 0, 0]^{\top}$ m/s (*hovering UAV*), $\mathbf{\Psi}^{\mathrm{AP}} = [110.0°, 20.0°, 20.0°]$, $\mathbf{C}^{\mathrm{UAV}\prime} = [0.4, 0.4, 0.4]^{\top}$, $t = 0$ s, $\sigma_A = 10.0°$, $F_1 = 5.0$ Hz, $F_2 = 25.0$ Hz.

Figs. 1–3 represent parameters that influence the phase shift. In the ACF, the phase shift is calculated as the ratio of the path length between the transmitting and receiving antennas to the wavelength. Therefore, it is expected that the correlation drops more quickly for shorter wavelengths, as shown in Fig. 1. However, it is important to note here that mmWave suffers much more from the increased effect of jittering, making the adoption of a solution to mitigate UAV fluctuations in mmWave systems essential. The amplitude of jitter and the distance from the antenna to the centroid introduce variations in the path lengths, as depicted in Fig. 4. These variations can be significant to induce a shift in the signal phase, consequently altering the ACF, as suggested by Theorem 2. Fig. 2 provides insights into the reduction in coherence time due to jitter, indicating that the interval in which the channel maintains 70.0% correlation for $\sigma_A = 3.0°$ is three times greater than that for $\sigma_A = 10.0°$. Additionally, we observe from Fig. 3, where $c = c_x = c_y = c_z$, that the distance from the antenna element to the centroid has an impact on the ACF by increasing the variation in path lengths during jitter. Therefore, the ACF may vary due to jittering, even if the UAV is hovering in the air. Furthermore, jittering can also influence the Doppler shift due to the radial velocity component that arises from the rotational movement [28].

The variation in the correlation of the LoS path is notably slower compared to that of the multipath, primarily due to the

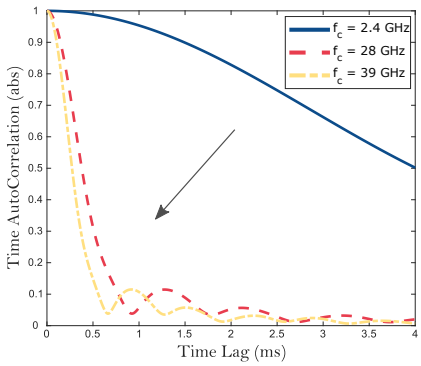

Fig. 1: Influence of the carrier frequency on jittering's impact on the normalized ACF.

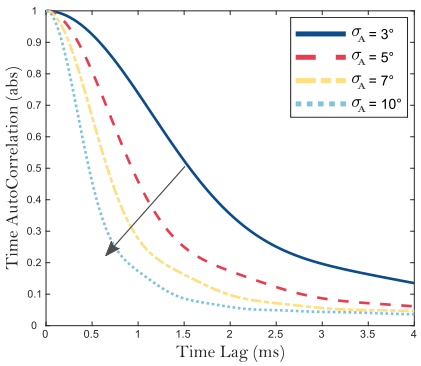

Fig. 2: Impact of the jittering amplitude on the normalized ACF.

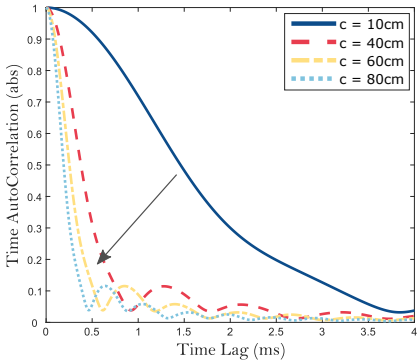

Fig. 3: Influence of the distance to the centroid on jittering's impact on the normalized ACF.

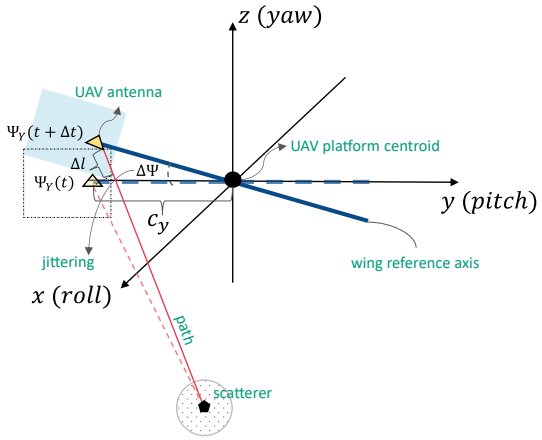

Fig. 4: Path length variation due to jitter.

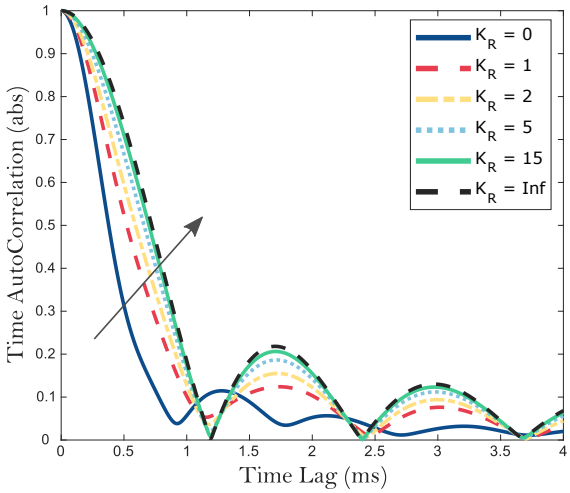

Fig. 5: Influence of the Rician factor on jittering's impact on the normalized ACF.

absence of overlapping phase-shifted signals. In Fig. 5, we examine the influence of the linear factor K_{R} on jittering. We observe that the absolute value of the ACF for the LoS path ($K_{\mathrm{R}} = \infty$) with jittering doesn't remain constant over time, unlike the ideal scenario. This variance stems from the phase shift's fluctuations over time caused by random changes in the antennas' attitude due to jitters. Additionally, we noticed that jittering has a lesser impact on LoS in comparison to NLoS, although it remains significant. This implies that the robustness of LoS can mitigate the influence of random jitter to some extent.

We now evaluate the performance of the proposed EKF for a moving and jittering UAV. We set the UAV velocity to $\mathbf{v}^{\mathrm{UAV}} = 10.0\boldsymbol{k}(45.0°, 7.5°)$ m/s. We adopt the spatially sparse precoding proposed in [47], along with the associated rate equation, considering an overhead of 10% for the simulation setup in Tab. II with a single discrete Fourier transform (DFT) codebook for uplink training and downlink data transmission. We consider $L = 4$ dominant paths[2]. Then we evaluate the rate as a function of the effective training signal-to-noise ratio (SNR)[3] for projected precoders concerning: ideal CSI (without estimation errors and aging), aged CSI (without estimation errors) in one time-slot, CSI predicted with EKF–AR(2) considering ACF with jittering (EKF-J), and without jittering (EKF). From Fig. 6 we can see an improvement of approximately 5.0 Mbps between the EKF-J and EKF solutions. Also, it is observed that even in poor SNR conditions, the EKF-J can still provide good performance. Note that EKF-J is constructed considering a more realistic ACF, thus not resulting in an increase in computational cost. Therefore, utilizing a more sophisticated ACF that incorporates the fluctuations of the UAV platform is crucial and essential for rate optimization.

V. Conclusion

The presence of fluctuations during the hovering and movement phases of a UAV can have significant implications for the time ACF and, as such, must be carefully considered during

[2]In a LoS scenario, we consider one LoS path and three NLoS paths.

[3]We define the effective SNR as the one that incorporates array gain in its calculation.

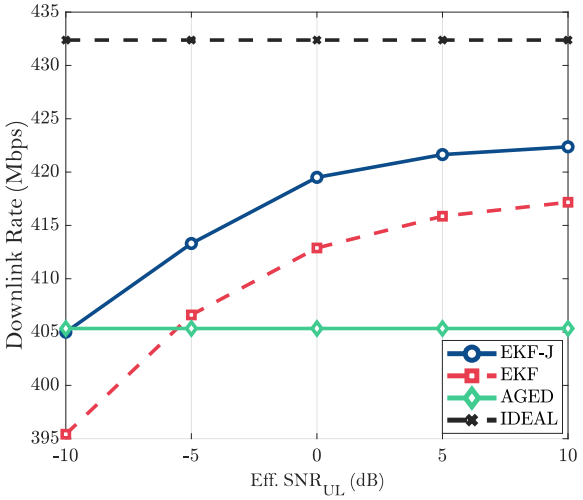

Fig. 6: Analysis and mitigation of the effect of jittering on the downlink rate.

SE optimization for ground-to-air communication. In practice, it is important to note that these effects will not be consistently intense but may occur suddenly with intensity due to factors that destabilize the UAV, such as wind gusts. This may result in data rate drops or even signal interruption, especially in mmWave frequencies or when there are direct line-of-sight obstructions. Mathematically, it is interesting to observe that if the center of the antenna array coincides with the centroid of the UAV platform, the variation in ACF due to UAV fluctuations can be considerably reduced. However, it is crucial to emphasize that, in practice, it may not always be feasible to install the antenna array at the exact centroid position of the UAV platform. This discrepancy between mathematical idealization and practical limitations should be considered when designing and implementing network-connected UAVs to ensure the robustness and reliability of ground-to-air communications. Finally, our proposal for an EKF-based channel predictor, designed to mitigate channel aging accentuated by UAV platform fluctuations, is viable and effective. The solution proposed for single-user MIMO can be extended to multi-user MIMO systems in small-cell and cell-free networks, where the impact of channel aging is particularly strong.

Appendix A
Proof of Approximate Channel Model

Proof of Theorem 1. Before proving it, we need to make some assumptions.

Let us consider the SBT path type, that is, an indirect link from the transmitter T to the s-th scatterer of the l-th cluster around T, denoted by S_{ls}, and from S_{ls} to R. From Fig. 7 we deduce the vector relations that will be used in the development of our GBSM. We define:

$$\begin{aligned}\overrightarrow{TR} &:= \mathbf{D}^{\mathrm{LoS}} = \|\mathbf{D}^{\mathrm{LoS}}\|_2 \boldsymbol{k}^{\mathrm{LoS}} ,\\ \overrightarrow{RS_{ls}} &:= \mathbf{D}^{\mathrm{RS}}_{ls} = \|\mathbf{D}^{\mathrm{RS}}_{ls}\|_2 \boldsymbol{k}^{\mathrm{TS}}_{ls} ,\\ \overrightarrow{TS_{ls}} &:= \mathbf{D}^{\mathrm{TS}}_{ls} = \|\mathbf{D}^{\mathrm{TS}}_{ls}\|_2 \boldsymbol{k}^{\mathrm{RS}}_{ls} ,\end{aligned} \tag{31}$$

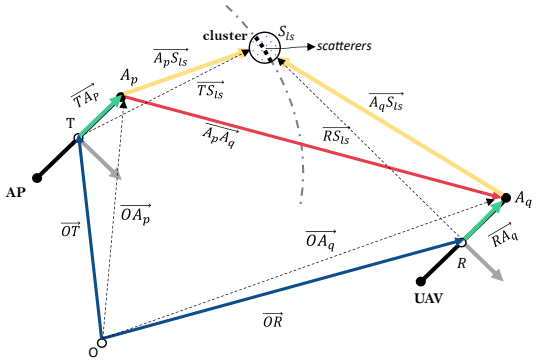

Fig. 7: Vector diagram of the 3D-GBSM channel (top view).

and

$$\begin{aligned}\boldsymbol{k}^{\mathrm{LoS}} &:= \boldsymbol{k}\left(\phi^{\mathrm{LoS}}, \theta^{\mathrm{LoS}}\right) ,\\ \boldsymbol{k}^{\mathrm{TS}}_{ls} &:= \boldsymbol{k}\left(\phi^{\mathrm{TS}}_{ls}, \theta^{\mathrm{TS}}_{ls}\right) ,\\ \boldsymbol{k}^{\mathrm{RS}}_{ls} &:= \boldsymbol{k}\left(\phi^{\mathrm{RS}}_{ls}, \theta^{\mathrm{RS}}_{ls}\right) ,\end{aligned}$$

where ϕ^{LoS}_{ls}, $\theta^{\mathrm{LoS}}_{ls}$, ϕ^{TS}_{ls}, $\theta^{\mathrm{TS}}_{ls}$, ϕ^{RS}_{ls} and $\theta^{\mathrm{RS}}_{ls}$ are the azimuth and elevation components of the LoS path, AoDs and AoAs of the NLoS paths, respectively, $\mathbf{D}$ is the distance vector between the specified points and $\|\cdot\|_2$ is the Euclidean distance.

Assumption 2. *For the LoS component and a given cluster l, the distance D, power $\eta(D^{-1})$ and Doppler frequency f_{d} of the link between the antennas change slowly enough to be considered constant over the time intervals of interest, so that there are variations only on a small scale:*

$$\eta^{\mathrm{LoS|SBT}}_{pq,ls}(t, D^{-1}) \approx \eta^{\mathrm{LoS|SBT}}_{pq,ls}(0, D^{-1}) := \eta^{\mathrm{LoS|SBT}}_{pq,ls}$$

and

$$\int_0^t f^{\mathrm{LoS|SBT}}_{\mathrm{d},pq,ls}\mathrm{d}t \approx t f^{\mathrm{LoS|SBT}}_{\mathrm{d},pq,ls} .$$

Assumption 3. *For sufficiently long distances, the influence of the size of the antenna array on the power and Doppler frequency can be neglected, so that:*

$$\eta^{\mathrm{LoS|SBT}}_{pq,ls} \approx \eta^{\mathrm{LoS|SBT}}_{ls} ,$$

$$f^{\mathrm{LoS}}_{\mathrm{d},pq} \approx \frac{\left\langle \mathbf{D}^{\mathrm{LoS}}, \mathbf{v}^{\mathrm{UAV}} \right\rangle}{\|\mathbf{D}^{\mathrm{LoS}}\|_2} = \langle \boldsymbol{k}^{\mathrm{LoS}}, \mathbf{v}^{\mathrm{UAV}} \rangle ,$$

$$f^{\mathrm{SBT}}_{\mathrm{d},pq,ls} \approx f^{\mathrm{TS}}_{\mathrm{d},ls} + f^{\mathrm{RS}}_{\mathrm{d},ls} = \frac{\left\langle \mathbf{D}^{\mathrm{RS}}_{ls}, \mathbf{v}^{\mathrm{UAV}} \right\rangle}{\left\|\mathbf{D}^{\mathrm{RS}}_{ls}\right\|_2} = \langle \boldsymbol{k}^{\mathrm{RS}}_{ls}, \mathbf{v}^{\mathrm{UAV}} \rangle ,$$

where $f^{\mathrm{TS}}_{\mathrm{d},ls} = 0$ for the static AP.

Assumption 4. *The distance from the antenna to the cluster is sufficiently greater than the greatest distance from the antenna element to the UAV centroid on the receiver side and greater than the size of the antenna array on the transmitter side.*

Consider a GBSM channel resulting from the overlap of L dominant paths of the LoS and NLoS-SBT types, where the latter can be a cluster of N_{S} scatterers. Aiming only at

the dimensions of space and time, the narrowband downlink channel response between a transmitter antenna element p and another receiver q is:

$$H_{pq}(t) = \sqrt{\frac{K_{\mathrm{R}}}{K_{\mathrm{R}}+1}} H_{pq}^{\mathrm{LoS}}(t) + \sqrt{\frac{1}{K_{\mathrm{R}}+1}} \sum_{l=2}^{L} \sum_{s=1}^{N_s} H_{pq,ls}^{\mathrm{SBT}}(t) \ ,$$

$$H_{pq}^{\mathrm{LoS}}(t) = \sqrt{\eta_{pq}^{\mathrm{LoS}}} \exp\left\{ \mathrm{j}\, \frac{2\pi}{\lambda} \int_0^t f_{\mathrm{d},pq}^{\mathrm{LoS}}(t)\mathrm{d}t - \mathrm{j}\, \frac{2\pi}{\lambda} \varphi_{pq}^{\mathrm{LoS}}(t) \right\} \ ,$$

$$H_{pq,ls}^{\mathrm{SBT}}(t) = \sqrt{\eta_{pq,ls}^{\mathrm{SBT}}} \exp\left\{ \mathrm{j}\, \frac{2\pi}{\lambda} \int_0^t f_{\mathrm{d},pq,ls}^{\mathrm{SBT}}(t)\mathrm{d}t - \mathrm{j}\, \frac{2\pi}{\lambda} \varphi_{pq,ls}^{\mathrm{SBT}}(t) \right\} \ ,$$

where f_{d} and φ represent the Doppler and phase shift, respectively, K_{R} denotes the Rician factor, and η denotes the power of each ray. In the equations above, we omitted the *initial phase* of the signal in the LoS component, as well as the *phase noise* in the NLoS components due to the effects of non-coherent electromagnetic reflection and dispersion.

We have that

$$\overrightarrow{A_p S_{ls}} = -\overrightarrow{TA_p} + \overrightarrow{TS_{ls}} \Rightarrow \mathbf{D}_{p,ls}^{\mathrm{TS}} = \mathbf{D}_{ls}^{\mathrm{TS}} - \mathbf{A_p}$$

and

$$\overrightarrow{A_q S_{ls}} = -\overrightarrow{RA_q} + \overrightarrow{RS_{ls}} \Rightarrow \mathbf{D}_{q,ls}^{\mathrm{RS}}(t) = \mathbf{D}_{ls}^{\mathrm{RS}} - \mathbf{A_q}(t) \ .$$

To model a path whose direction starts from the transmitting antenna p and ends at the receiving antenna q, we invert the direction of the $\overrightarrow{A_q S_{ls}}$ vector, such that:

$$\mathbf{D}_{q,ls}^{\mathrm{RS}}(t) = \mathbf{D}_{ls}^{\mathrm{RS}} + \mathbf{A_q}(t) \ .$$

Let us then consider that:

$$\|\mathbf{D}_{ls}^{\mathrm{TS}}\|_2 \gg \|\mathbf{A_p}\|_2 \ , \qquad \|\mathbf{D}_{ls}^{\mathrm{RS}}\|_2 \gg \|\mathbf{A_q}(t)\|_2 \ .$$

Using a linear approximation based on a first-order Taylor series, we obtain:

$$\|\mathbf{D}_{p,ls}^{\mathrm{TS}}\|_2 \approx \|\mathbf{D}_{ls}^{\mathrm{TS}}\|_2 - \langle \mathbf{A_p}, \boldsymbol{k}_{ls}^{\mathrm{TS}} \rangle$$

and

$$\|\mathbf{D}_{q,ls}^{\mathrm{RS}}(t)\|_2 \approx \|\mathbf{D}_{ls}^{\mathrm{RS}}\|_2 + \langle \mathbf{A_q}(t), \boldsymbol{k}_{ls}^{\mathrm{RS}} \rangle \ .$$

So, the phase shift of the channel response is:

$$\varphi_{pq,ls}^{\mathrm{SBT}}(t) \approx \|\mathbf{D}_{ls}^{\mathrm{TS}}\|_2 + \|\mathbf{D}_{ls}^{\mathrm{RS}}\|_2 - \langle \mathbf{A_p}, \boldsymbol{k}_{ls}^{\mathrm{TS}} \rangle + \langle \mathbf{A_q}(t), \boldsymbol{k}_{ls}^{\mathrm{RS}} \rangle \ .$$

We can factorize the frequency response of the H_{pq} subchannel into its transmitter and receiver components:

$$\begin{aligned} H_{pq,ls}^{\mathrm{SBT}}(t) &= \sqrt{\eta_{pq,ls}^{\mathrm{SBT}}} \exp\left\{ \mathrm{j}\, \frac{2\pi}{\lambda} \int_0^t f_{\mathrm{d},pq,ls}^{\mathrm{SBT}}(t)\mathrm{d}t \right\} \\ &\quad \times \exp\left\{ -\mathrm{j}\, \frac{2\pi}{\lambda} \varphi_{pq,ls}^{\mathrm{SBT}}(t) \right\} \\ &\approx \sqrt{\eta_{pq,ls}^{\mathrm{SBT}}} \exp\left\{ \mathrm{j}\, \frac{2\pi}{\lambda} t f_{\mathrm{d},ls}^{\mathrm{SBT}} \right\} \\ &\quad \times \exp\left\{ -\mathrm{j}\, \frac{2\pi}{\lambda} \left(\|\mathbf{D}_{ls}^{\mathrm{TS}}\|_2 + \|\mathbf{D}_{ls}^{\mathrm{RS}}\|_2 \right) \right\} \\ &\quad \times \exp\left\{ -\mathrm{j}\, \frac{2\pi}{\lambda} \langle \mathbf{A_q}(t), \boldsymbol{k}_{ls}^{\mathrm{RS}} \rangle \right\} \exp\left\{ -\mathrm{j}\, \frac{2\pi}{\lambda} \langle \mathbf{A_p}, \boldsymbol{k}_{ls}^{\mathrm{TS}} \rangle \right\}^* \ , \end{aligned}$$

then our spatial signature can be simplified with the normalized steering vector so that:

$$\mathbf{a}(\phi,\theta,t) = \frac{1}{\sqrt{N_{\mathrm{A}}}} \left[\mathrm{a}_1(\phi,\theta,t), \mathrm{a}_2(\phi,\theta,t), \ldots, \mathrm{a}_{N_{\mathrm{AN}}}(\phi,\theta,t) \right]^\top \ ,$$

with

$$\mathrm{a}_{p(q)}(\theta,\phi,t) = \exp\left(-\mathrm{j}\, \frac{2\pi}{\lambda} \mathbf{A_{p(q)}}(t)^\top \boldsymbol{k}(\theta,\phi) \right) \ .$$

The downlink MIMO channel matrix can then be obtained by:

$$H_{pq,ls}^{\mathrm{SBT}}(t) \approx g_{ls}^{\mathrm{SBT}}(t) \mathrm{a}_q\left(\phi_{ls}^{\mathrm{RS}}, \theta_{ls}^{\mathrm{RS}}, t\right) \mathrm{a}_p^*\left(\phi_{ls}^{\mathrm{TS}}, \theta_{ls}^{\mathrm{TS}}\right) \ ,$$

and

$$\mathbf{H}_{ls}^{\mathrm{SBT}}(t) \approx g_{ls}^{\mathrm{SBT}}(t) \mathbf{a}_{\mathrm{UAV}}\left(\phi_{ls}^{\mathrm{RS}}, \theta_{ls}^{\mathrm{RS}}, t\right) \mathbf{a}_{\mathrm{AP}}^\dagger\left(\phi_{ls}^{\mathrm{TS}}, \theta_{ls}^{\mathrm{TS}}\right) \ ,$$

such that the SBT complex gain is

$$\begin{aligned} g_{ls}^{\mathrm{SBT}}(t) = &\sqrt{\eta_{ls}^{\mathrm{SBT}}} \exp\left\{ -\mathrm{j}\, \frac{2\pi}{\lambda} \left(\|\mathbf{D}_{ls}^{\mathrm{TS}}\|_2 + \|\mathbf{D}_{ls}^{\mathrm{RS}}\|_2 \right) \right\} \\ &\times \exp\left\{ \mathrm{j}\, \frac{2\pi}{\lambda} t f_{\mathrm{d},ls}^{\mathrm{SBT}} \right\} \ . \end{aligned}$$

Assumption 5. *For SBT path type and scatterers' cylindrical distribution of radius R_{AP}, let us consider the following distances:*

$$\|\mathbf{D}_{ls}^{\mathrm{TS}}\|_2 = R_{\mathrm{AP}} |\sec\theta_{ls}^{\mathrm{TS}}| \ ,$$

and considering that $\|\mathbf{D}^{\mathrm{LoS}}\|_2 \gg \|\mathbf{D}_{ls}^{\mathrm{TS}}\|_2$, it follows that

$$\begin{aligned} \|\mathbf{D}_{ls}^{\mathrm{RS}}\|_2 &= \|\mathbf{D}^{\mathrm{LoS}} - \mathbf{D}_{ls}^{\mathrm{TS}}\|_2 \\ &\approx \|\mathbf{D}^{\mathrm{LoS}}\|_2 - R_{\mathrm{AP}} |\sec\theta_{ls}^{\mathrm{TS}}| \langle \boldsymbol{k}_{ls}^{\mathrm{TS}}, \boldsymbol{k}^{\mathrm{LoS}} \rangle \ , \end{aligned}$$

such that $\mathbf{D}^{\mathrm{LoS}} = \mathbf{D}^{\mathrm{UAV}} - \mathbf{D}^{\mathrm{AP}}$.

The LoS component test follows the same procedure as the NLoS proof. These channel models can be simulated based on sum-of-sinusoids (SoS) [38].

□

APPENDIX B
PROOF OF AUTOCORRELATION FUNCTION

Proof of Theorem 2. We adopt the following formula for each cluster l:

$$Q_{pq,\widetilde{p}\widetilde{q}}(t;\Delta t) = \mathbb{E}\left[H_{pq}(t+\Delta t) H_{\widetilde{p}\widetilde{q}}^*(t) \right] \ ,$$

where the expectation is calculated relative to the scatterer s from the cluster l. For the NLoS components, it turns out that:

$$\begin{aligned} &H_{pq,ls}^{\mathrm{SBT}}(t+\Delta t) H_{\widetilde{p}\widetilde{q},ls}^{\mathrm{SBT}\,*}(t) \approx g_{ls}^{\mathrm{SBT}}(t+\Delta t) g_{ls}^{\mathrm{SBT}\,*}(t) \\ &\times \mathrm{a}_q\left(\phi_{ls}^{\mathrm{RS}}, \theta_{ls}^{\mathrm{RS}}, t+\Delta t\right) \mathrm{a}_{\widetilde{q}}^*\left(\phi_{ls}^{\mathrm{RS}}, \theta_{ls}^{\mathrm{RS}}, t\right) \\ &\times \mathrm{a}_p^*\left(\phi_{ls}^{\mathrm{TS}}, \theta_{ls}^{\mathrm{TS}}\right) \mathrm{a}_{\widetilde{p}}\left(\phi_{ls}^{\mathrm{TS}}, \theta_{ls}^{\mathrm{TS}}\right) \ . \end{aligned} \tag{32}$$

Assumption 6. *The number of scatterers (rays) within a cluster is infinite and cylindrically distributed according to the following independent PDFs:*

$$\begin{aligned} &\mathrm{pdf}\left(\phi_{ls}\right) = \frac{e^{\kappa \cos\left(\phi_{ls} - \bar{\phi}_l\right)}}{2\pi I_0(\kappa)}, \quad \phi_1 \le \phi_{ls} \le \phi_2 \quad \textit{von Mises PDF} \\ &\mathrm{pdf}\left(\theta_{ls}\right) = \frac{\pi}{4\theta_{\mathrm{m}}} \cos\left(\frac{\pi}{2} \frac{\theta_{ls} - \bar{\theta}_l}{\theta_{\mathrm{m}}} \right), \quad \theta_1 \le \theta_{ls} \le \theta_2 \quad \textit{cosine PDF} \end{aligned} \tag{33}$$

where $I_0(\cdot)$ is the zeroth-order modified Bessel function of the first kind, κ and θ_{m} regulate the intra-cluster angular standard deviation, while $\bar{\phi}_l$ and $\bar{\theta}_l$ denote the angular mean. For a model without spatial restrictions, one can do: $\phi_1 = -\pi$, $\phi_2 = \pi$, $\theta_1 = |\theta_{ls} - \bar{\theta}_l|$ and $\theta_2 = \pi/2$.

In the case of scatterers distributed around the AP, we adopt the following notation: κ_{AP} and θ_{mAP}. The PDFs above has been used for both AoAs and AoDs [35].

We define:

$$\begin{aligned}
&\mathrm{a}^{\mathrm{TS}}_{p\widetilde{p},ls} \coloneqq \mathrm{a}_p\left(\phi^{\mathrm{TS}}_{ls},\theta^{\mathrm{TS}}_{ls}\right)\mathrm{a}^{*}_{\widetilde{p}}\left(\phi^{\mathrm{TS}}_{ls},\theta^{\mathrm{TS}}_{ls}\right)\\
&\mathrm{a}^{\mathrm{RS}}_{q\widetilde{q},ls}(t,\Delta t) \coloneqq \mathrm{a}_q\left(\phi^{\mathrm{RS}}_{ls},\theta^{\mathrm{RS}}_{ls},t+\Delta t\right)\mathrm{a}^{*}_{\widetilde{q}}\left(\phi^{\mathrm{RS}}_{ls},\theta^{\mathrm{RS}}_{ls},t\right)\\
&g^{\mathrm{SBT}}_{ls}(t,\Delta t) \coloneqq g^{\mathrm{SBT}}_{ls}(t+\Delta t)g^{\mathrm{SBT}\,*}_{ls}(t)\ ,
\end{aligned}$$

then, for a single cylindrical distribution, it follows that:

$$\begin{aligned}
&Q^{\mathrm{SBT}}_{pq,\widetilde{p}\widetilde{q}}(t;\Delta t)\\
&=\frac{1}{L}\sum_{l=1}^{L}\lim_{N_{\mathrm{S}}\to\infty}\frac{1}{N_{\mathrm{S}}}\sum_{s=1}^{N_{\mathrm{S}}}\mathbb{E}\left[g^{\mathrm{SBT}}_{ls}(t,\Delta t)\mathrm{a}^{\mathrm{TS}\,*}_{p\widetilde{p},ls}\mathrm{a}^{\mathrm{RS}}_{q\widetilde{q},ls}(t,\Delta t)\right]\\
&=\frac{1}{L}\sum_{l=1}^{L}\int_{\phi_1^{\mathrm{TS}}}^{\phi_2^{\mathrm{TS}}}\int_{\theta_1^{\mathrm{TS}}}^{\theta_2^{\mathrm{TS}}}\int_{\Theta_\Psi} g^{\mathrm{SBT}}_{ls}(t,\Delta t)\mathrm{a}^{\mathrm{TS}\,*}_{p\widetilde{p},ls}\mathrm{a}^{\mathrm{RS}}_{q\widetilde{q},ls}(t,\Delta t)\\
&\times \mathrm{pdf}\left(\boldsymbol{\vartheta}_\Psi\right)\mathrm{pdf}\left(\theta^{\mathrm{TS}}_{ls}\right)\mathrm{pdf}\left(\phi^{\mathrm{TS}}_{ls}\right)\mathrm{d}\boldsymbol{\vartheta}_\Psi\mathrm{d}\theta^{\mathrm{TS}}_{ls}\mathrm{d}\phi^{\mathrm{TS}}_{ls}\ ,
\end{aligned}\tag{34}$$

where in the last equality, the Law of the Unconscious Statistician and the assumption that the number of scatterers is infinite were applied. The Θ_Ψ is the space of parameters $\boldsymbol{\vartheta}_\Psi$ of the random process (13), which refers to the attitude fluctuation models considered within the product of the array response $\mathrm{a}^{\mathrm{RS}}_{q\widetilde{q},ls}(t,\Delta t)$. Note that ϕ^{RS}_{ls} and $\theta^{\mathrm{RS}}_{ls}$ must be written as a function of ϕ^{TS}_{ls} and $\theta^{\mathrm{TS}}_{ls}$. Furthermore, the independence between ϕ_{ls} and θ_{ls} is valid for the cylindrical scattering model. In the case of spherical models, joint PDFs must be considered. The expression in (34) does not have a closed form, but can be solved numerically.

Regarding the array's response, it turns out:

$$\begin{aligned}
&\mathrm{a}_q(\phi^{\mathrm{RS}}_{ls},\theta^{\mathrm{RS}}_{ls},t+\Delta t)\\
&=\exp\left\{-j\mathbf{A}^{\top}_{\mathbf{q}}(t+\Delta t)\boldsymbol{k}^{\mathrm{RS}}_{ls}\right\}\\
&=\exp\left\{-\mathrm{j}\,\frac{2\pi}{\lambda}\mathbf{A}'^{\top}_{\mathbf{q}}\mathbf{R}^{\top}(t+\Delta t)\boldsymbol{k}^{\mathrm{RS}}_{ls}\right\}\\
&=\exp\left\{-\mathrm{j}\,\frac{2\pi}{\lambda}\mathbf{A}'^{\top}_{\mathbf{q}}\left(\mathbf{R}(t)+\dot{\mathbf{R}}(t)\Delta\Psi_{\Delta t}\right)^{\top}\boldsymbol{k}^{\mathrm{RS}}_{ls}\right\}\\
&=\exp\left\{-\mathrm{j}\,\frac{2\pi}{\lambda}\mathbf{A}'^{\top}_{\mathbf{q}}\mathbf{R}(t)^{\top}\boldsymbol{k}^{\mathrm{RS}}_{ls}\right\}\\
&\times\exp\left\{-\mathrm{j}\,\frac{2\pi}{\lambda}\Delta\Psi_{\Delta t}\mathbf{A}'^{\top}_{\mathbf{q}}\dot{\mathbf{R}}(t)^{\top}\boldsymbol{k}^{\mathrm{RS}}_{ls}\right\}\ .
\end{aligned}$$

Then:

$$\begin{aligned}
&\mathrm{a}^{\mathrm{RS}}_{q\widetilde{q},ls}(t,\Delta t)=\exp\left\{-\mathrm{j}\,\frac{2\pi}{\lambda}\mathbf{A}^{\top}_{\mathbf{q}}(t)\boldsymbol{k}^{\mathrm{RS}}_{ls}\right\}\exp\left\{\mathrm{j}\,\frac{2\pi}{\lambda}\mathbf{A}^{\top}_{\widetilde{\mathbf{q}}}(t)\boldsymbol{k}^{\mathrm{RS}}_{ls}\right\}\\
&\times\exp\left\{-\mathrm{j}\,\frac{2\pi}{\lambda}\Delta\Psi_{\Delta t}\mathbf{A}'^{\top}_{\mathbf{q}}\dot{\mathbf{R}}(t)^{\top}\boldsymbol{k}^{\mathrm{RS}}_{ls}\right\}\\
&=\exp\left\{-\mathrm{j}\,\frac{2\pi}{\lambda}\left(\mathbf{A}_{\mathbf{q}}(t)-\mathbf{A}_{\widetilde{\mathbf{q}}}(t)\right)^{\top}\boldsymbol{k}^{\mathrm{RS}}_{ls}\right\}\\
&\times\exp\left\{-\mathrm{j}\,\frac{2\pi}{\lambda}\Delta\Psi_{\Delta t}\mathbf{A}'^{\top}_{\mathbf{q}}\dot{\mathbf{R}}(t)^{\top}\boldsymbol{k}^{\mathrm{RS}}_{ls}\right\}\ .
\end{aligned}$$

Regarding the gain, neglecting the variation in distance due to the UAV movement in a small time interval Δt, we have:

$$g^{\mathrm{SBT}}_{ls}(t,\Delta t)=\eta^{\mathrm{SBT}}_{ls}\exp\left\{\mathrm{j}\,\frac{2\pi}{\lambda}f^{\mathrm{SBT}}_{\mathrm{d},ls}\Delta t\right\}\ .$$

For $p=\widetilde{p}$ or $q=\widetilde{q}$, it results in ACF:

$$\begin{aligned}
&\mathbb{E}\left[g^{\mathrm{SBT}}_{ls}(t,\Delta t)\mathrm{a}^{\mathrm{RS}}_{qq,ls}(t,\Delta t)\mathrm{a}^{\mathrm{TS}\,*}_{pp,ls}\right]\\
&=\eta^{\mathrm{SBT}}_{l}\mathbb{E}\left[\exp\left\{\mathrm{j}\,\frac{2\pi}{\lambda}\Delta t\langle\boldsymbol{k}^{\mathrm{RS}}_{ls},\mathbf{v}^{\mathrm{UAV}}\rangle\right\}\right.\\
&\left.\times\exp\left\{-\mathrm{j}\,\frac{2\pi}{\lambda}\Delta\Psi_{\Delta t}\mathbf{A}'^{\top}_{\mathbf{q}}\dot{\mathbf{R}}(t)^{\top}\boldsymbol{k}^{\mathrm{RS}}_{ls}\right\}\right]\ .
\end{aligned}$$

The demonstration for the LoS path follows the same procedure.

□

REFERENCES

[1] G. Geraci, A. Garcia-Rodriguez, M. M. Azari, A. Lozano, M. Mezzavilla, S. Chatzinotas, Y. Chen, S. Rangan, and M. D. Renzo, "What will the future of UAV cellular communications be? a flight from 5G to 6G," *IEEE Commun. Surveys Tuts.*, vol. 24, no. 3, pp. 1304–1335, 2022. doi: 10.1109/COMST.2022.3171135

[2] A. S. Abdalla and V. Marojevic, "Communications standards for unmanned aircraft systems: The 3GPP perspective and research drivers," *IEEE Commun. Stand. Mag.*, vol. 5, no. 1, pp. 70–77, 2021. doi: 10.1109/MCOMSTD.001.2000032

[3] R. Bajracharya, R. Shrestha, S. Kim, and H. Jung, "6G NR-U based wireless infrastructure UAV: Standardization, opportunities, challenges and future scopes," *IEEE Access (J.)*, vol. 10, pp. 30 536–30 555, 2022. doi: 10.1109/ACCESS.2022.3159698

[4] K. Meng, Q. Wu, J. Xu, W. Chen, Z. Feng, R. Schober, and A. L. Swindlehurst, "UAV-enabled integrated sensing and communication: Opportunities and challenges," *IEEE Wireless Commun.*, pp. 1–9, 2023. doi: 10.1109/MWC.131.2200442

[5] X. Lin, V. Yajnanarayana, S. D. Muruganathan, S. Gao, H. Asplund, H.-L. Maattanen, M. Bergstrom, S. Euler, and Y.-P. E. Wang, "The sky is not the limit: LTE for unmanned aerial vehicles," *IEEE Commun. Mag.*, vol. 56, no. 4, pp. 204–210, 2018. doi: 10.1109/MCOM.2018.1700643

[6] Y. Zeng, J. Lyu, and R. Zhang, "Cellular-connected UAV: Potential, challenges, and promising technologies," *IEEE Wireless Commun.*, vol. 26, no. 1, pp. 120–127, 2019. doi: 10.1109/MWC.2018.1800023

[7] E. Björnson, J. Hoydis, and L. Sanguinetti, "Massive MIMO networks: Spectral, energy, and hardware efficiency," *Found. Trends Signal Process. (J.)*, ch. 2, vol. 11, no. 3-4, p. 154–655, 2017. doi: 10.1561/2000000093

[8] Y. M. Tsang and A. S. Poon, "Detecting human blockage and device movement in mmWave communication system," in *Proc. IEEE Globecom Workshops (GC Wkshps)*, 2011. doi: 10.1109/GLOCOM.2011.6134444 pp. 1–6.

[9] A. Papazafeiropoulos, "Impact of hardware impairments and channel aging millimeter-wave heterogeneous networks," in *Proc. of IEEE WCNC*, 2019. doi: 10.1109/WCNC.2019.8885847 pp. 1–7.

[10] L. Thiele, M. Olbrich, M. Kurras, and B. Matthiesen, "Channel aging effects in CoMP transmission: gains from linear channel prediction," in *Proc. of ASILOMAR*, 2011. doi: 10.1109/ACSSC.2011.6190359 pp. 1924–1928.

[11] K. T. Truong and R. W. Heath, "Effects of channel aging in massive MIMO systems," *J. Commun. Networks*, vol. 15, no. 4, pp. 338–351, 2013. doi: 10.1109/JCN.2013.000065

[12] B. H. Wang, D. B. Wang, Z. A. Ali, B. Ting Ting, and H. Wang, "An overview of various kinds of wind effects on unmanned aerial vehicle," *Meas. Control (J.)*, vol. 52, no. 7-8, pp. 731–739, 2019. doi: 10.1177/0020294019847688

[13] W. H. Semke and M. D. Dunlevy, "A review of the vibration environment onboard small unmanned aircraft," in *Proc. of IMAC*. Springer, 2019. doi: 10.1007/978-3-319-74642-5_18 pp. 155–164.

[14] P. Abichandani, D. Lobo, G. Ford, D. Bucci, and M. Kam, "Wind measurement and simulation techniques in multi-rotor small unmanned aerial vehicles," *IEEE Access (J.)*, vol. 8, pp. 54 910–54 927, 2020. doi: 10.1109/ACCESS.2020.2977693

[15] D. Mishra and E. Natalizio, "A survey on cellular-connected UAVs: Design challenges, enabling 5G/B5G innovations, and experimental advancements," *Comput. Netw. (J.)*, vol. 182, p. 107451, 2020. doi: 10.1016/j.comnet.2020.107451

[16] C. Zhang, W. Zhang, W. Wang, L. Yang, and W. Zhang, "Research challenges and opportunities of UAV millimeter-wave communications," *IEEE Wireless Commun.*, vol. 26, no. 1, pp. 58–62, 2019. doi: 10.1109/MWC.2018.1800214

[17] Z. Xiao, P. Xia, and X.-g. Xia, "Enabling UAV cellular with millimeter-wave communication: potentials and approaches," *IEEE Commun. Mag.*, vol. 54, no. 5, pp. 66–73, 2016. doi: 10.1109/MCOM.2016.7470937

[18] D. Xu, Y. Sun, D. W. K. Ng, and R. Schober, "Robust resource allocation for UAV systems with UAV jittering and user location uncertainty," in *Proc. IEEE Globecom Workshops (GC Wkshps)*, 2018. doi: 10.1109/GLOCOMW.2018.8644086 pp. 1–6.

[19] H. Wu, Y. Wen, J. Zhang, Z. Wei, N. Zhang, and X. Tao, "Energy-efficient and secure air-to-ground communication with jittering UAV," *IEEE Trans. Veh. Technol.*, vol. 69, no. 4, pp. 3954–3967, 2020. doi: 10.1109/TVT.2020.2971520

[20] C. Lu and P. Chen, "Robust channel estimation scheme for multi-UAV mmWave MIMO communication with jittering," *Electronics (J.)*, vol. 12, no. 9, p. 2102, 2023. doi: 10.3390/electronics12092102

[21] J. Zhao, F. Gao, W. Jia, W. Yuan, and W. Jin, "Integrated sensing and communications for UAV communications with jittering effect," *IEEE Wireless Commun. Lett.*, vol. 12, no. 4, pp. 758–762, 2023. doi: 10.1109/LWC.2023.3243590

[22] M. T. Dabiri, H. Safi, S. Parsaeefard, and W. Saad, "Analytical channel models for millimeter wave UAV networks under hovering fluctuations," *IEEE Trans. Wireless Commun.*, vol. 19, no. 4, pp. 2868–2883, 2020. doi: 10.1109/TWC.2020.2968530

[23] Z. Ma, B. Ai, R. He, G. Wang, Y. Niu, M. Yang, J. Wang, Y. Li, and Z. Zhong, "Impact of UAV rotation on MIMO channel characterization for air-to-ground communication systems," *IEEE Trans. Veh. Technol.*, vol. 69, no. 11, pp. 12 418–12 431, 2020. doi: 10.1109/TVT.2020.3028301

[24] M. Banagar, H. S. Dhillon, and A. F. Molisch, "Impact of UAV wobbling on the air-to-ground wireless channel," *IEEE Trans. Veh. Technol.*, vol. 69, no. 11, pp. 14 025–14 030, 2020. doi: 10.1109/TVT.2020.3026975

[25] B. Yang and W. Zhang, "Analysis of propagation characteristics for MIMO air-to-air communications with UAV jitter," in *Proc. International Symposium on Antennas, Propagation and EM Theory (ISAPE)*, vol. 1, 2021. doi: 10.1109/ISAPE54070.2021.9753118 pp. 1–4.

[26] X. Yang, D. Zhai, R. Zhang, H. Cao, S. Garg, and G. Kaddoum, "Impact of UAV 3D wobbles on the non-stationary air-to-ground channels at sub-6 GHz bands," in *Proc. IEEE Globecom Workshops (GC Wkshps)*, 2022. doi: 10.1109/GLOBECOM48099.2022.10000615 pp. 4473–4478.

[27] W. Wang and W. Zhang, "Jittering effects analysis and beam training design for UAV millimeter wave communications," *IEEE Trans. Wireless Commun.*, vol. 21, no. 5, pp. 3131–3146, 2022. doi: 10.1109/TWC.2021.3118558

[28] S. Yang, Z. Zhang, J. Zhang, and J. Zhang, "Impact of rotary-wing UAV wobbling on millimeter-wave air-to-ground wireless channel," *IEEE Trans. Veh. Technol.*, vol. 71, no. 9, pp. 9174–9185, 2022. doi: 10.1109/TVT.2022.3181334

[29] J. Zheng, J. Zhang, E. Björnson, and B. Ai, "Impact of channel aging on cell-free massive MIMO over spatially correlated channels," *IEEE Trans. Wireless Commun.*, vol. 20, no. 10, pp. 6451–6466, 2021. doi: 10.1109/TWC.2021.3074421

[30] A. R. L. Paiva, G. Fodor, W. C. Freitas, Y. C. Silva, and C. F. e Silva, "Kalman-filter-based tracking of millimeter-wave channel parameters for V2X applications," in *IEEE Conf. Stand. Commun. Networking (CSCN)*. IEEE, 2019. doi: 10.1109/CSCN.2019.8931350 pp. 1–7.

[31] H. Q. Ngo, A. Ashikhmin, H. Yang, E. G. Larsson, and T. L. Marzetta, "Cell-free massive MIMO versus small cells," *IEEE Trans. Wireless Commun.*, vol. 16, no. 3, pp. 1834–1850, 2017. doi: 10.1109/TWC.2017.2655515

[32] R. Pinto Antonioli, I. M. Braga, G. Fodor, Y. C. B. Silva, A. L. F. de Almeida, and W. C. Freitas, "On the energy efficiency of cell-free systems with limited fronthauls: Is coherent transmission always the best alternative?" *IEEE Trans. Wireless Commun.*, vol. 21, no. 10, pp. 8729–8743, 2022. doi: 10.1109/TWC.2022.3169114

[33] F. Kaltenberger, H. Jiang, M. Guillaud, and R. Knopp, "Relative channel reciprocity calibration in MIMO/TDD systems," in *Future Netw. Mob. Summit (Conf.)*, 2010. doi: 20.500.12708/71399 pp. 1–10.

[34] R. W. Heath, N. González-Prelcic, S. Rangan, W. Roh, and A. M. Sayeed, "An overview of signal processing techniques for millimeter wave MIMO systems," *IEEE J. Sel. Topics Signal Process.*, vol. 10, no. 3, pp. 436–453, 2016. doi: 10.1109/JSTSP.2016.2523924

[35] X. Cheng, Y. Li, C.-X. Wang, X. Yin, and D. W. Matolak, "A 3D geometry-based stochastic model for unmanned aerial vehicle MIMO ricean fading channels," *IEEE Internet Things J.*, vol. 7, no. 9, pp. 8674–8687, 2020. doi: 10.1109/JIOT.2020.2995707

[36] Q. Zhu, Y. Wang, K. Jiang, X. Chen, W. Zhong, and N. Ahmed, "3D non-stationary geometry-based multi-input multi-output channel model for UAV-ground communication systems," *IET Microw. Antennas Propag.*, vol. 13, no. 8, pp. 1104–1112, 2019. doi: 10.1049/iet-map.2018.6129

[37] E. T. Michailidis and A. G. Kanatas, "Three-dimensional HAP-MIMO channels: Modeling and analysis of space-time correlation," *IEEE Trans. Veh. Technol.*, vol. 59, no. 5, pp. 2232–2242, 2010. doi: 10.1109/TVT.2010.2042629

[38] A. G. Zajic and G. L. Stuber, "Three-dimensional modeling and simulation of wideband MIMO mobile-to-mobile channels," *IEEE Trans. Wireless Commun.*, vol. 8, no. 3, pp. 1260–1275, 2009. doi: 10.1109/TWC.2009.070379

[39] B. Yang, K. Letaief, R. Cheng, and Z. Cao, "Channel estimation for OFDM transmission in multipath fading channels based on parametric channel modeling," *IEEE Trans. Commun.*, vol. 49, no. 3, pp. 467–479, 2001. doi: 10.1109/26.911454

[40] J. Lee, G.-T. Gil, and Y. H. Lee, "Exploiting spatial sparsity for estimating channels of hybrid MIMO systems in millimeter wave communications," in *Proc. IEEE Globecom Workshops (GC Wkshps)*, 2014. doi: 10.1109/GLOCOM.2014.7037320 pp. 3326–3331.

[41] K. Baddour and N. Beaulieu, "Autoregressive modeling for fading channel simulation," *IEEE Trans. Wireless Commun.*, vol. 4, no. 4, pp. 1650–1662, 2005. doi: 10.1109/TWC.2005.850327

[42] J. He, T. Kim, H. Ghauch, K. Liu, and G. Wang, "Millimeter wave MIMOchannel tracking systems," in *Proc. IEEE Globecom Workshops (GC Wkshps)*, 2014. doi: 10.1109/GLOCOMW.2014.7063467 pp. 416–421.

[43] M. H. C. Garcia, A. Molina-Galan, M. Boban, J. Gozalvez, B. Coll-Perales, T. Şahin, and A. Kousaridas, "A tutorial on 5G NR V2X communications," *IEEE Commun. Surveys Tuts.*, vol. 23, no. 3, pp. 1972–2026, 2021. doi: 10.1109/COMST.2021.3057017

[44] M. R. Akdeniz, Y. Liu, M. K. Samimi, S. Sun, S. Rangan, T. S. Rappaport, and E. Erkip, "Millimeter wave channel modeling and cellular capacity evaluation," *IEEE J. Sel. Areas Commun.*, vol. 32, no. 6, pp. 1164–1179, 2014. doi: 10.1109/JSAC.2014.2328154

[45] M. Alonzo, S. Buzzi, A. Zappone, and C. D'Elia, "Energy-efficient power control in cell-free and user-centric massive MIMO at millimeter wave," *IEEE Trans. Green Commun. Netw.*, vol. 3, no. 3, pp. 651–663, 2019. doi: 10.1109/TGCN.2019.2908228

[46] G. Femenias and F. Riera-Palou, "Cell-free millimeter-wave massive MIMO systems with limited fronthaul capacity," *IEEE Access (J.)*, vol. 7, pp. 44 596–44 612, 2019. doi: 10.1109/ACCESS.2019.2908688

[47] O. E. Ayach, S. Rajagopal, S. Abu-Surra, Z. Pi, and R. W. Heath, "Spatially sparse precoding in millimeter wave MIMO systems," *IEEE Trans. Wireless Commun.*, vol. 13, no. 3, pp. 1499–1513, 2014. doi: 10.1109/TWC.2014.011714.130846

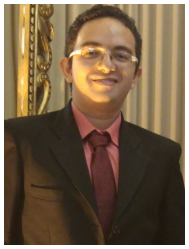

A. Regilane L. Paiva received the B.Sc. and M.Sc. degrees in teleinformatics engineering from the Federal University of Ceará (UFC), Fortaleza, Brazil, in 2016 and 2018, respectively. He currently holds a Research Engineer position with the Wireless Telecom Research Group (GTEL), UFC, where he works on projects in technical and scientific cooperation with Ericsson Research. Has experience with backend web development. His main research interests include statistical signal processing and machine learning solutions for wireless communication systems, millimeter waves and wireless channel models.

Walter C. Freitas Jr received the B.S. and M.S. degrees in electrical engineering from the Federal University of Ceará, Fortaleza, Brazil, and the Ph.D. degree in teleinformatic engineering from the Federal University of Ceará, in 2006. During his studies, he was supported by the Brazilian Agency FUNCAP and Ericsson. During Q3 of 2015 up to Q2 of 2016, he was a Postdoc Researcher with I3S/CNRS Laboratory, from the University of Nice, Sophia Antipolis, France. During 2005 Walter Freitas Jr. was a Senior Research of the Nokia Technology Institute, He is currently an Assistant Professor with the Department of Teleinformatics Engineering of the Federal University of Ceará and Researcher of Wireless Telecom Research Group one of the most important research groups in telecommunication in Brazil. His main research interests include features development to improve the performance of the wireless communication systems, interference avoidance tools, multilinear algebra, and tensor-based signal processing applied to communications.

Yuri C. B. Silva received the B.Sc. and M.Sc. degrees in electrical engineering from the Federal University of Ceará, Fortaleza, Brazil, in 2002 and 2004, respectively, and the Dr.-Ing. degree in electrical engineering from the Technische Universität Darmstadt, Darmstadt, Germany, in 2008. From 2001 to 2004 he was with the Wireless Telecom Research Group (GTEL), Fortaleza, Brazil. In 2003 he was a Visiting Researcher at Ericsson Research, Stockholm, Sweden. From 2005 to 2008, he was with the Communications Engineering Laboratory of the Technische Universität Darmstadt. He is currently an Associate Professor with the Federal University of Ceará and Researcher at GTEL. He also holds a productivity fellowship in technological development and innovation from CNPq. His main research interests include wireless communications systems, multi-antenna processing, interference management, multicast services, and cooperative communications.

Roberto P. Antonioli received the B.Sc. degree in teleinformatics engineering (magna cum laude) from the Federal University of Ceará (UFC), Fortaleza, Brazil, in 2016, and the M.Sc. and Ph.D. degrees in teleinformatics engineering also from UFC in 2017 and 2020, respectively. In 2021, Roberto's Ph.D thesis was selected the best Electrical Engineering PhD Thesis in Brazil in the context of an annual prize issued by CAPES (Brazilian agency that supports graduate programs). He currently holds a Post-doc. position with the Wireless Telecom Research Group (GTEL), UFC, where he works on projects in technical and scientific cooperation with Ericsson Research. He is also a Software Developer with Hewlett Packard, Brazil. In 2018/2019, he was a Visiting Researcher with Ericsson Research, Sweden. His research interests include 5G wireless communication networks with multiple radio access technologies and multi-connectivity, and also scheduling algorithms for QoS provision.

Gábor Fodor (Senior Member, IEEE) received the Ph.D. degree in electrical engineering from the Budapest University of Technology and Economics, Budapest, Hungary, in 1998, the Docent degree from the KTH Royal Institute of Technology, Stockholm, Sweden, in 2017, and the D.Sc. degree from the Hungarian Academy of Sciences (Doctor of MTA), Budapest, in 2019. He is currently a Master Researcher with Ericsson Research and an Adjunct Professor with the KTH Royal Institute of Technology. He has authored or coauthored more than 100 refereed journal articles and conference papers and seven book chapters and holds more than 100 European and U.S.-granted patents. From 2017 to 2020, he was a member of the board of the IEEE Sweden Joint Communications, Information Theory, and Vehicle Technology Chapter. He was a co-recipient of the IEEE Communications Society Stephen O. Rice Prize in 2018 and the Best Student Conference Paper Award from the IEEE Sweden VT/COM/IT Chapter in 2018. He has served as the Chair of the Full-Duplex Emerging Technology Initiative of the IEEE Communications Society from 2019 to 2021. He is currently serving as an Editor for IEEE Transactions on Wireless Communications and IEEE Wireless Communications.